



UNIVERSITY OF LEEDS

This is a repository copy of *Suitability of electrochemical test methods for evaluating corrosion of the steel in alkali activated slag concretes*.

White Rose Research Online URL for this paper:

<https://eprints.whiterose.ac.uk/189618/>

Version: Accepted Version

---

**Article:**

Ma, Q, Bai, Y, Yang, C et al. (2 more authors) (2022) Suitability of electrochemical test methods for evaluating corrosion of the steel in alkali activated slag concretes. Magazine of Concrete Research, 74 (24). pp. 1259-1269. ISSN 0024-9831

<https://doi.org/10.1680/jmacr.21.00089>

---

This is protected by copyright. All rights reserved. This is an author produced version of an article published in Magazine of Concrete Research. Uploaded in accordance with the publisher's self-archiving policy.

**Reuse**

Items deposited in White Rose Research Online are protected by copyright, with all rights reserved unless indicated otherwise. They may be downloaded and/or printed for private study, or other acts as permitted by national copyright laws. The publisher or other rights holders may allow further reproduction and re-use of the full text version. This is indicated by the licence information on the White Rose Research Online record for the item.

**Takedown**

If you consider content in White Rose Research Online to be in breach of UK law, please notify us by emailing [eprints@whiterose.ac.uk](mailto:eprints@whiterose.ac.uk) including the URL of the record and the reason for the withdrawal request.



# Magazine of Concrete Research

## **Suitability of electrochemical test methods for evaluating corrosion of the steel in alkali activated slag concretes**

MACR-2021-089-R1 | Paper: materials research

Submitted on: 06-12-21

Submitted by: Qianmin Ma, Yun Bai, Changhui Yang, Muhammed Basheer, Sreejith Nanukuttan

Keywords: ALKALI-ACTIVATED-SLAG, CORROSION, GRAVIMETRIC-MASS-LOSS, MACROCELL-CORROSION-CURRENT, HALF-CELL-POTENTIAL



# Suitability of electrochemical test methods for evaluating corrosion of the steel in alkali activated slag concretes

Qianmin Ma<sup>a&b</sup>, Yun Bai<sup>c</sup>, Changhui Yang<sup>d</sup>, P. A. Muhammed Basheer<sup>e</sup> and Sreejith V.

Nanukuttan<sup>b\*</sup>

<sup>a</sup> Faculty of Civil Engineering and Mechanics, Kunming University of Science and Technology; Yunnan Provincial Key Laboratory of Civil Engineering Disaster Prevention, Jingming South Road, 650500 Kunming, China

<sup>b</sup> School of Natural and Built Environment, Queen's University Belfast, University Road Belfast, BT7 1NN, Northern Ireland, UK

<sup>c</sup> Department of Civil, Environmental & Geomatic Engineering, University College London, Gower Street, London, WC1E 6BT, UK

<sup>d</sup> College of Material Science and Engineering, Chongqing University, 174 Shapingba Main Street, 400044, China

<sup>e</sup> School of Civil Engineering, University of Leeds, England, LS2 9JT, UK

\*Corresponding author's email: s.nanukuttan@qub.ac.uk

## Abstract

The electrochemical tests commonly used for evaluating reinforcement corrosion in PC-based concretes may not be appropriate for testing alkali activated slag (AAS) systems due to its different pore structure and pore solution composition. In this article, corrosion behaviour of the steel bars in 12 AAS concrete mixes with different alkali concentration and modulus of sodium silicate solution was monitored by using gravimetric mass loss measurement. The

results obtained from other electrochemical tests were compared to the gravimetric mass loss to determine their suitability for assessing the corrosion of steel in AAS concretes. It was found that only 7.8-28% of the mass loss was accounted by the macrocell current for AAS concretes, indicating that this type of test underestimates the corrosion of the steel in AAS. The steel bars in the AAS concretes gave a much higher negative half-cell potential value, presumably due to the influence of sulphides. In summary, it has been established that the criteria for assessing the onset and progress of corrosion of steel in PC concretes is not suitable for the same purpose in the range of AAS concretes studied.

**Key words:** alkali activated slag, corrosion of steel, gravimetric mass loss, macrocell corrosion current, half-cell potential

## 1. Introduction

Reinforcement steel in concrete is protected from harmful substances by a passive layer of iron oxide film. Steel corrosion is known to commence when this film breaks down. The alkalinity and nature of ions in concrete pores at the steel-concrete interface have a significant influence on the stability of this passive film and therefore the initiation of corrosion (Glasser, 1991 and Broomfield, 2007). Corrosion of steel in concrete is an electrochemical process involving the formation of anodic and cathodic regions. The progress of corrosion depends on the rate of generation of electrons and ions as well as the ease of flow of these between the anode and the cathode (Broomfield, 2007). Amongst them one of the most significant factors is the ease of movement of hydroxyl ions generated at the cathodic region to the anodic region through the pore solution (Broomfield, 2007).

Alkali activated slag (AAS) is manufactured by activating ground granulated blast furnace slag (GGBS) using an alkali activator (such as sodium silicate solution) (Shi, *et al.*, 2006). Due to the nature of the raw materials, i.e., slag and alkaline activators, the pore solution chemistry and pore structure are different from that of Portland cement (PC) based concretes (Shi, *et al.*, 2006, Torres-Carrasco, *et al.*, 2015, Ma, *et al.*, 2016). Different alkali concentrations ( $\text{Na}_2\text{O}\%$  of mass of slag) and modulus ( $M_s$ ) of sodium silicate solution will also influence the pore solution/structure (Ma, *et al.*, 2016, Al-Otaibi, 2008, Ravikumar and Neithalath, 2013). Previously, the chloride diffusivity and bulk electrical resistivity of various AAS systems were studied and it was found that they have low diffusivity and high bulk resistivity (Ma, *et al.*, 2016, Al-Otaibi, 2008, Ravikumar and Neithalath, 2013, Tennakoon, *et al.*, 2017), despite having a conductive pore solution. This would indicate a high resistance for the flow of ions from cathode to anode, so naturally a low rate of corrosion is expected. Further, the conductive pore solution and the nature of ions present in activated slag might interfere with the electrochemical test measurement.

Therefore, there is a need to assess whether there exists any variation between electrochemical measurements and actual corrosion of steel in AAS concretes and how can the criteria used for qualifying the corrosion resistance of PC concretes be used for AAS concretes. Recently, Criado and Provis (2018), Runci and Serdar (2020) and You *et al.* (2020) have demonstrated the corrosion behaviour of steel bars in AAS mortars under chloride environment. In the work by Criado and Provis (2018), a higher current density and a very negative corrosion potential were obtained for AAS system, while there was no visible rust on the surface of the bars embedded. Other researchers (Runci and Serdar, 2020, You. *et al.*, 2020) also confirmed that AAS system showed a low chloride diffusion and a high chloride binding capacity, and then a clean surface of the bars embedded. However, a more negative corrosion potential was obtained

for such system. A systematic study was, therefore, carried out using 12 different AAS concretes when the gravimetric method of assessing the corrosion was compared with electrochemical methods, such as half-cell potential measurements and macrocell corrosion currents. The results of this study are reported in this paper and recommendations are provided for assessing the onset and rate of corrosion of steel in AAS concretes using electrochemical methods.

## 2. Experimental programme

As stated above, the quantification of corrosion of reinforcing steel bars in 12 AAS concrete mixes with different Na<sub>2</sub>O% and Ms was measured by using gravimetric mass loss measurement. Corrosion current and half-cell potential of the steel bars were measured using a macrocell test set-up. The results were compared to the gravimetric mass loss to determine the suitability of these two electrochemical measurements for assessing (or quantifying) corrosion behaviour of the steel bars in the AAS concretes.

### 2.1 Materials

Ground Granulated Blast-furnace Slag (GGBS) provided by Civil and Marine Ltd., U. K. was used to manufacture all the AAS concretes. Class 42.5N PC conforming to British Standard EN 197-1 (2000) provided by Quinn group Ltd., U. K. was used to manufacture the PC control concrete. The chemical composition and physical properties of both the GGBS and the PC are reported in Table 1. In addition, sulphide content in the GGBS is 0.80% and chloride contents in the GGBS and the PC are 0.02% and 0.01%, respectively.

**Table 1** Chemical composition and physical properties of the GGBS and the PC

	CaO	SiO <sub>2</sub>	Al <sub>2</sub> O <sub>3</sub>	MgO	MnO	Fe <sub>2</sub> O <sub>3</sub>	K <sub>2</sub> O	Na <sub>2</sub> O	TiO <sub>2</sub>	SO <sub>3</sub>	LOI	Specific surface area (m <sup>2</sup> /kg)	Specific gravity
<b>GGBS</b>	39.4	34.3	15.0	8.00	0.50	0.40	0.38	0.45	0.70	--	0.05	527	2.90
<b>PC</b>	61.3	23.0	6.15	1.80	--	2.95	0.68	0.22	--	2.50	1.40	286	3.16

Sodium silicate solution (or commonly known as water glass, WG) with Na<sub>2</sub>O% of 12.45 and SiO<sub>2</sub>% of 43.60, which is available as ‘Crystal 0503’ from Charles Tennant & CO (NI) Ltd., U. K. was used as the activator for GGBS. Industrial grade sodium hydroxide powder with a purity of 99% supplied by Charles Tennant & CO (NI) Ltd., U. K. was used to adjust the Ms to the required values.

A barium based retarder ‘YP-1’® (Yang and Pu, 1993) was used in the AAS concretes to control their setting. The retarder was dry-blended with GGBS before mixing. The superplasticiser used in the PC concrete mix was CHEMCRETE HP3 provided by Larsen. It is a polycarboxylic polymer based superplasticiser with a water content of 40%, which was considered in proportioning the mixing water.

Crushed basalt from local sources in Northern Ireland with size fractions of 20mm and 10mm combined in a ratio of 1:1 was used as the coarse aggregate. Natural sand with fineness modulus of 2.53 was used as the fine aggregate. Water from the mains water supply was used to mix and cure the concretes (regime of curing is to be detailed in section 2.3).

## 2.2 Mix proportions

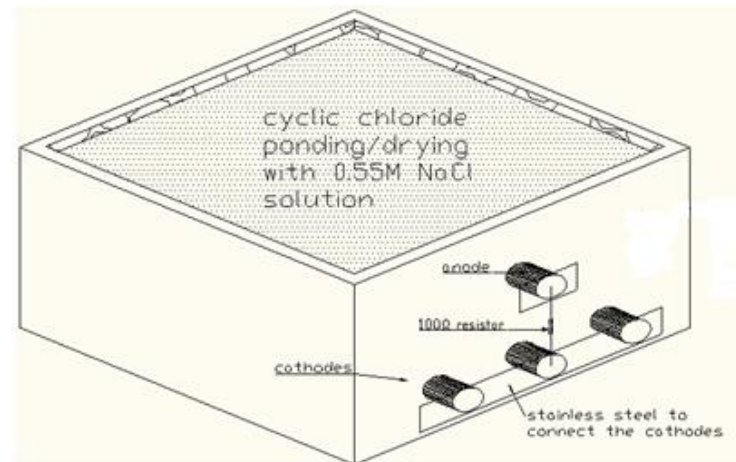
Twelve AAS concrete mixes with Na<sub>2</sub>O% of 4, 6, and 8 and Ms of WG of 0.75, 1.00, 1.50 and 2.00 were investigated. The total binder content, which is the sum of GGBS and solid component in the WG, was kept constant at 400kg/m<sup>3</sup> for all mixes. The water-binder ratio (W/B) was constant at 0.47 for all the AAS concretes. The water content in the WG was considered in proportioning the mixing water. The retarder with dosage of 0.3% of the mass of GGBS was used to retard the setting of the AAS concretes.

For the purpose of comparison, one PC concrete mix was manufactured with the same total binder content as that of the AAS concretes. A W/B of 0.42 was determined for the PC concrete to guarantee its compliance to British Standards EN 206-1 (2000) for the exposure environments of XS3 and XD3. The use of superplasticiser at 0.4% of mass of cement allowed the PC concrete to just achieve the minimum value of conforming to class of S2 (50mm) specified in British Standard EN 206-1 (2000).

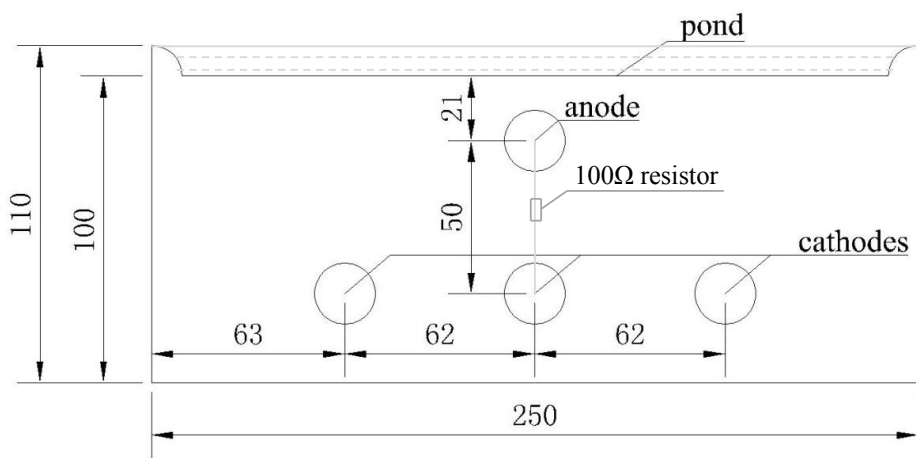
The ratio of fine aggregate to total aggregates was 36%, which was kept the same for both the PC and the AAS concretes.

### 2.3 Preparation of test specimens

Three 250×250×110mm blocks with a dyke on the top surface (as shown in Fig. 1) for each mix were cast for the tests to be detailed in section 2.4. For each block, four steel bars of diameter of 12mm and a length of 300mm were used to form the anode and the cathode, as shown in Fig. 1. Before embedding, the steel bars were cleaned with a wire brush and a dry cleaning cloth and then weighed. The procedure of preparation of the steel bars for macrocell corrosion test set-up is shown in Fig. 2. Approximately, 75mm of the steel bars at both ends were shielded from exposure environment (i.e., from corrosion) by applying two layers of self-amalgamating tape. Further, a rich mortar cover with a thickness of 5mm was applied over the tape. Then a layer of epoxy painting was applied onto the mortar cover. This ensured that exposure to penetrating chlorides was confined to a known area in the middle of the steel bars.



(a) Test specimen



(b) Cross-section view of the concrete block in mm

**Fig. 1.** A sketch of the macrocell corrosion test specimen showing the location of anode, cathode and the chloride pond



(a) Steel bars

(b) Steel bars wrapped in self-amalgamating tape  
at both ends(c) Casting mortar on top of self-amalgamating  
tape at one end(d) Casting mortar on top of the self-amalgamating  
tape at the other end



(e) Steel bars with mortar end caps



(f) Epoxy painted mortar end caps



(g) Cathodic and anodic bars embedded in the mould for casting test blocks

**Fig. 2.** Procedure of the preparation of the steel bars before embedding in test blocks and bars in the mould for casting test blocks

The concrete blocks were cast by following the procedure given in British Standard 1881-125 (1986), in three layers with each layer receiving sufficient compaction using a table vibrator before progressing to the next layer. Further to vibration, the surface layer was finished using a metal float. The moulds were covered with thick polythene sheets to minimise evaporation of

water from the surface of concrete. Approximately 1-hour after the concrete surface hardened, the moulds were covered with layers of previously wetted hessian and polythene sheet outer layer. The samples were stored in this condition for 3 days at an average temperature of  $20(\pm 2)^\circ\text{C}$ . The hessian was maintained at wet state by spraying water at every 6 hours. At the end of 3 days, the concrete specimens were demoulded, wrapped in both wet hessian and plastic bags and stored in a constant temperature room at  $20(\pm 1)^\circ\text{C}$  for 91 days. The hessian was rewetted if needed at every 2 weeks during the storage period.

In addition to the blocks for studying the corrosion, nine cubes of 100mm size were also cast for each mix by following the procedure described above.

## 2.4 Test procedure

### 2.4.1 Slump and compressive strength tests

The consistence of the concrete was measured by carrying out the slump test as per British Standard EN 12350-2 (2009). Three cubes each from the nine cubes cast for each mix were tested at the age of 3, 28 and 91 days to determine the compressive strength according to British Standard EN 12350-3 (2009).

### 2.4.2 Corrosion tests

One month before the test age of 91 days, the concrete blocks were moved to a constant temperature of  $23\pm 3^\circ\text{C}$  and relative humidity ( $55\pm 2\%$ ) chamber for conditioning the blocks for moisture for two weeks. Layers of epoxy paint were applied onto all of the surfaces of the blocks except the top surface used for ponding and the opposite bottom surface to allow the trapped air to escape. After coating the surfaces with the epoxy paint, the blocks were stored in the same conditioning room for another two weeks. Further, the anode and the cathodes was

electrically connected using a  $100\Omega$  resistor, as shown in Fig. 1. During the whole conditioning and test periods, the blocks were supported by two timber strips with a thickness of approximately 13mm so to allow air flow under the blocks. It was assumed that the test specimens did not carbonate during the period of moisture conditioning, except maybe the top 1mm, and did not interfere with the chloride transport during the ponding regime. Approximately 200ml 0.55M NaCl solution was ponded on the blocks for 1 day, which was then removed and the blocks were allowed to dry for 6 days. This cycle of ponding and drying was continued until the end of the test (~250 days). Before each ponding cycle began, half-cell potential of the anodic steel bars (at three locations from the central region of the bars) and electrical potential between the anode and the cathodes was measured by using a Cu/CuSO<sub>4</sub> half-cell apparatus and a voltmeter, respectively. Macrocell current through the circuit and further corrosion current density are calculated by using the equations below, respectively:

$$i_{mac} = \frac{1000 \cdot V}{R} \quad (1)$$

$$I_{corr} = \frac{i_{mac}}{A} \quad (2)$$

where,  $i_{mac}$  is macrocell current,  $\mu A$ ;  $V$  is the measured electrical potential, mV;  $R$  is the electrical resistance between anodic steel and cathodic steel,  $100\Omega$ ;  $I_{corr}$  is corrosion current density,  $\mu A/cm^2$  and  $A$  is the surface area of the steel bars (in  $cm^2$ ), which was available for exposure to chlorides and chloride induced corrosion.

The mass loss of anodic steel bar in a macrocell corrosion set-up is estimated using the following equation:

$$m = \frac{Q \cdot M}{F \cdot z} \quad (3)$$

in which,

$$Q = \int_0^t i_{mac} dt \quad (4)$$

where,  $m$  is mass loss of the steel, g;  $Q$  is charge passed, coulomb (notated by C);  $M$  is molar mass of steel, 56g/mol;  $F$  is Faraday's constant, 96485 coulombs/mol;  $z$  is valency of Fe, 2,  $i_{mac}$  is macrocell current, A (the  $\mu$ A from Eq.1 was converted A for using in Eq. 4) and  $t$  is time, s.

At the end of ponding, an area in the middle of the concrete blocks was profile ground in layers of 3mm depth to obtain concrete dust for the chloride analysis. Samples were collected up to the location of the anodic steel; that is, up to approximately 15mm from exposed surface. The total and water soluble chloride content in the dust samples was measured by using RILEM TC 178-TMC (2002a and 2002b). Further, the blocks were split opened to remove the anodic steel bars, which were then scrubbed with wire brush, wiped with a dry cloth and weighed to determine the mass loss caused by the corrosion.

#### 2.4.3 pH measurement

After removing the anodic bars, the concrete blocks were profile ground to collect dust samples from the depths of 3mm, 6mm, 9mm, 12mm, 15mm, 20mm, 25mm, 30mm, 35mm, 40mm and 45mm. Five gram ( $\pm 0.0001$ g) of the dust sample was then dissolved in 50 millilitre of deionised water in a glass beaker by stirring the content of 3 minutes. The pH of this suspension was measured using a pH meter, which is reported as apparent pH. The apparent pH was plotted against the depth to obtain the pH profile at the end of the cyclic ponding test.

### 3. Results and discussion

#### 3.1 Slump and compressive strength

The slump and compressive strength of all the 13 mixes were reported in our previous paper (Ma, *et al.*, 2016) which are reported here in Table 2. As stated earlier, a retarder of 0.3% by mass of slag was used for the AAS mixes whilst superplasticiser of 0.5% by mass of cement was used for PC mix. The water-binder ratio of the AAS concretes was 0.47 whereas it was 0.42 for the PC concrete.

As reported in the previous paper (Ma, *et al.*, 2016), all the mixes satisfied the minimum slump of 50mm for their use in marine environments (British Standard 8500-1, 2006). However, it was found that the addition of the retarder and the use of slightly higher water-binder ratio in the AAS concretes had a slightly detrimental effect on the compressive strength, particularly at the age of 3d. The mixes were expected to meet the requirement for XS3 and XD3 exposure environments specified in British Standard EN 206-1 (2000) as the PC reference concrete was designed to satisfy this requirement. The compressive strength at the age of 28 days suggests that not all the AAS concretes achieved the required strength of 58MPa for the two exposure classes. However, most of the AAS concretes met the strength requirement of 50MPa for the exposure classes XS1, XD1 and XD2. At the time of carrying out this research, a suitable admixture that could be used to control the workability of the AAS concretes was not available, but it is expected that with the availability of new admixtures specifically for use with AAS and geopolymers from different manufacturers, the above limitation could be addressed.

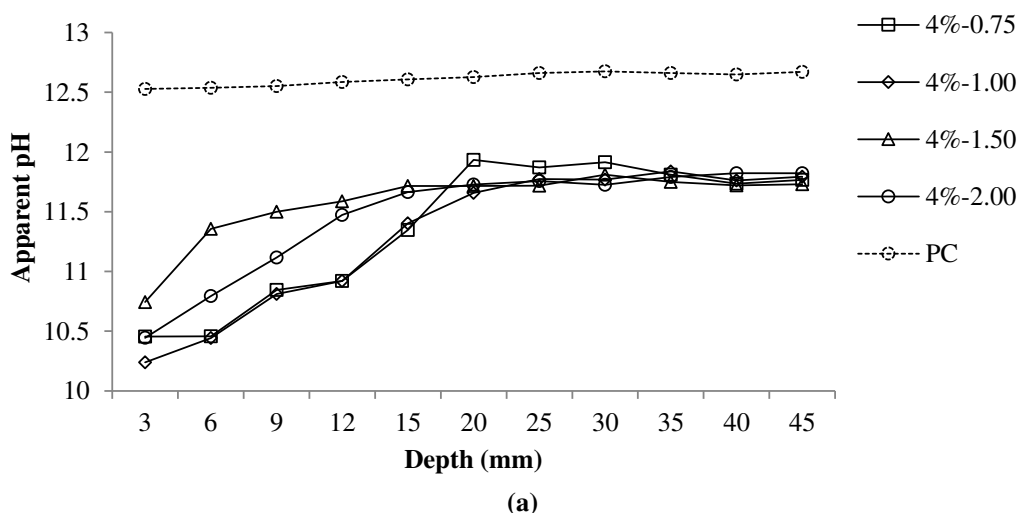
**Table 2** Slump and compressive strength ( $\pm$  standard deviation) of the concrete mixes

Mix ID (Na <sub>2</sub> O% -Ms)	Slump (mm)	Compressive strength (MPa)		
		3 day	28 day	91 day
4%-0.75	55	22.3 $\pm$ 0.1	44.7 $\pm$ 0.2	46.4 $\pm$ 1.0
4%-1.00	55	21.8 $\pm$ 0.1	46.7 $\pm$ 1.0	55.6 $\pm$ 0.6
4%-1.50	55	1.7 $\pm$ 0.0	49.5 $\pm$ 0.2	52.6 $\pm$ 2.3
4%-2.00	55	1.4 $\pm$ 0.0	33.3 $\pm$ 0.4	44.1 $\pm$ 0.1
6%-0.75	65	31.7 $\pm$ 0.7	47.3 $\pm$ 0.0	51.8 $\pm$ 2.4
6%-1.00	65	37.3 $\pm$ 0.2	53.6 $\pm$ 0.0	59.1 $\pm$ 0.8
6%-1.50	65	20.3 $\pm$ 0.7	60.8 $\pm$ 0.1	67.4 $\pm$ 2.6
6%-2.00	75	8.0 $\pm$ 0.0	59.6 $\pm$ 0.2	68.7 $\pm$ 2.1
8%-0.75	70	32.3 $\pm$ 0.0	51.9 $\pm$ 0.1	56.2 $\pm$ 0.2
8%-1.00	105	32.7 $\pm$ 2.4	53.6 $\pm$ 0.1	67.1 $\pm$ 0.6
8%-1.50	145	34.1 $\pm$ 0.7	59.3 $\pm$ 3.2	70.5 $\pm$ 2.5
8%-2.00	180	11.7 $\pm$ 0.2	55.4 $\pm$ 0.2	65.0 $\pm$ 0.8
PC	50	35.4 $\pm$ 1.2	58.9 $\pm$ 1.8	66.3 $\pm$ 2.3

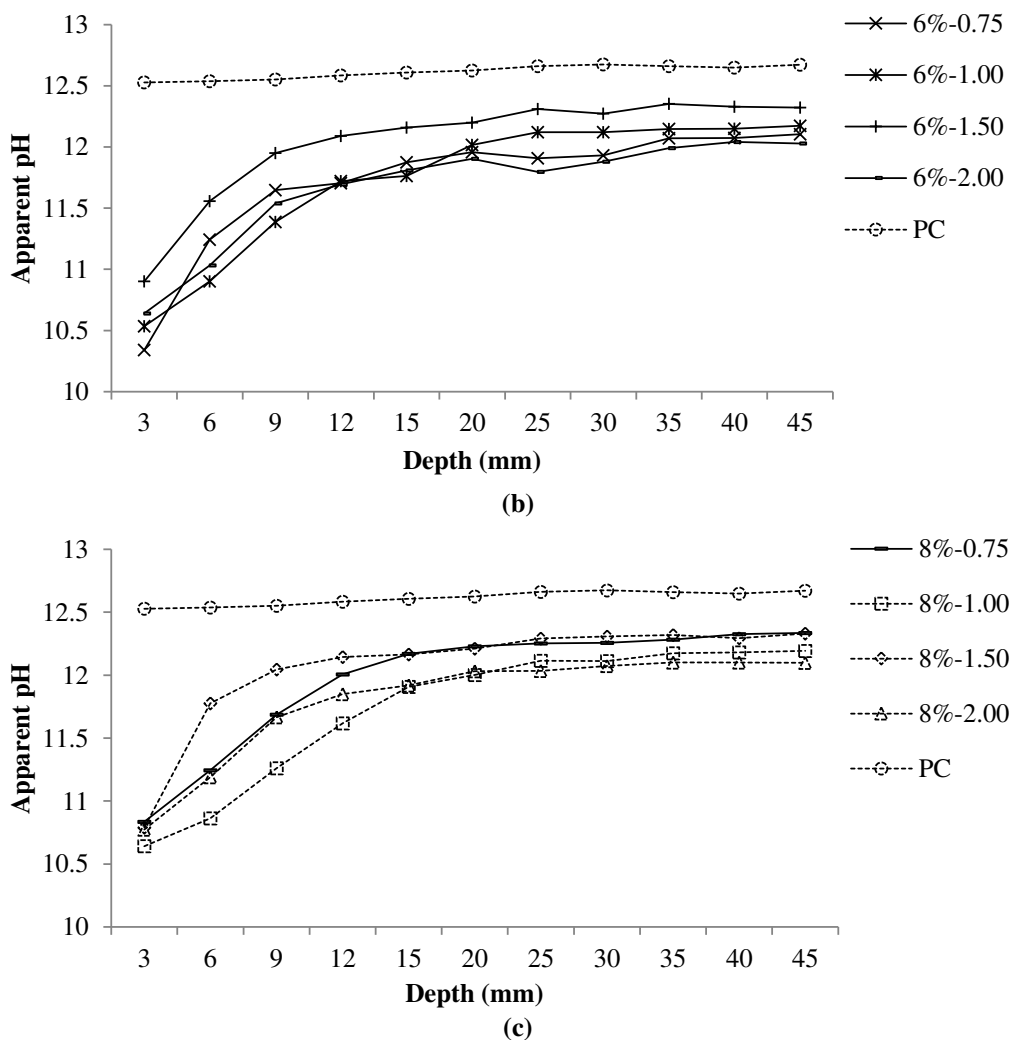
### 3.2 Apparent pH

Fig. 3 shows the apparent pH profiles of concretes after the cyclic ponding test. It can be seen that the alkalinity of the AAS concretes was considerably lower in the surface zone (15mm) compared to the PC concrete. This reduction is considered to have been caused by the outward diffusion of alkaline materials from the AAS concretes and the partial carbonation of the near surface of concrete during the conditioning stage before exposing to chlorides. As the

concentration of sodium ions in the exposure solution was high, the outward diffusion of sodium ions from AAS concretes could not have happened. Therefore, the outward diffusion of potassium, calcium and hydroxyl ions is mainly responsible for the reduction in alkalinity. However,  $\text{Ca}(\text{OH})_2$  is not one of the hydration products of the AAS concretes. Therefore, the continuous outward diffusion of the alkaline materials in AAS concretes could also result in the dissolution of the hydration products of the AAS concretes, such as C-S-H gels (Johannesson, *et al.*, 2007), which was confirmed in this study with the presence of exposed aggregates at the end of the ponding test. In the PC concrete,  $\text{Ca}(\text{OH})_2$  would dissolve in the pore solution to buffer the alkalinity when the outward diffusion of alkaline materials occurs, resulting in the trend seen in Fig. 3.



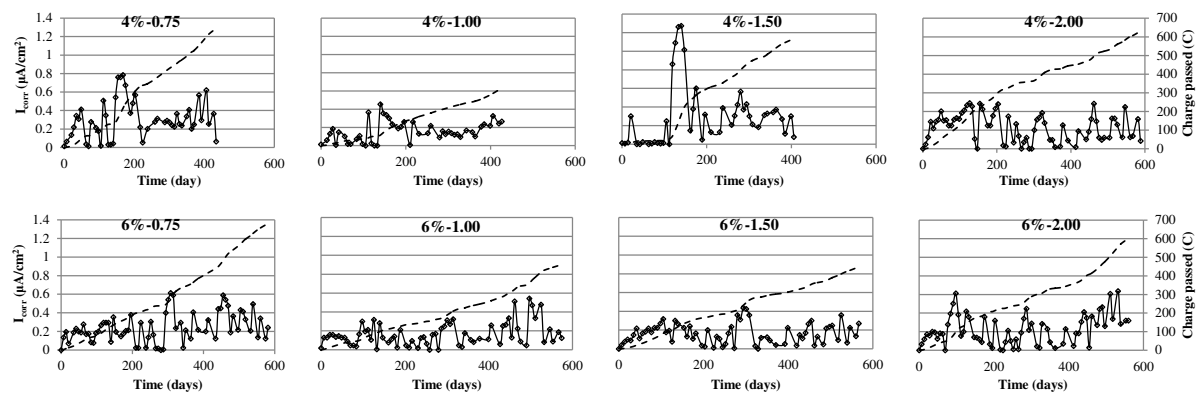
(a)



**Fig. 3** Apparent pH profiles of the concretes after the cyclic ponding test (the anodic steel bar was at 15mm depth in all cases)

### 3.3 Macrocell current

Fig. 4 presents the evolution of corrosion current density ( $\mu\text{A}/\text{cm}^2$ ) and the charge passed (Coulomb - C) for the 12 AAS concretes and the PC reference concrete.



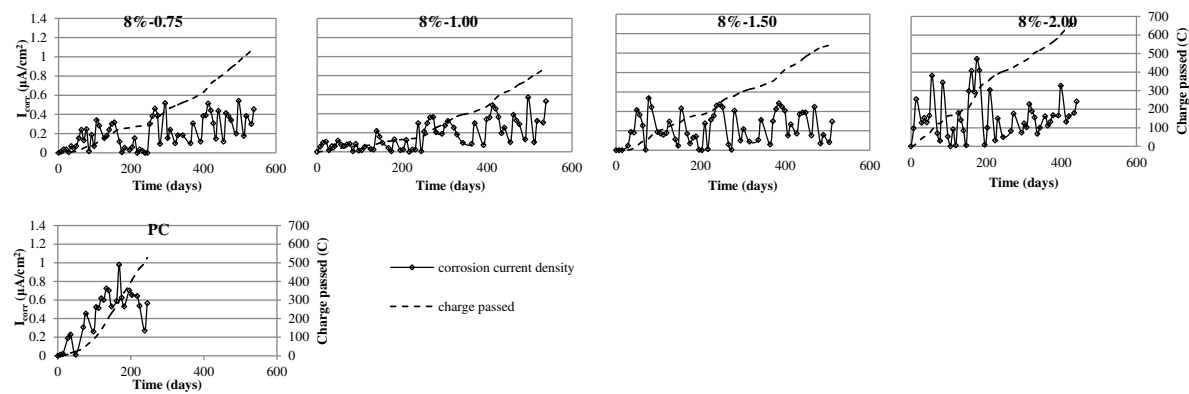


Fig. 4 Corrosion current and charge passed

From Fig. 4 it can be seen that the corrosion current for AAS concrete fluctuates highly, but in general stays lower than that of the PC reference concrete. There is no prolonged initiation period for any of the mixes studied, presumably due to the fairly aggressive cyclic ponding regime and the lower cover depth of 15mm used in this research. The relatively lower alkalinity (Fig. 3) and higher sulphide concentration of the AAS concretes (Ma, *et al.*, 2016) could have disrupted the passive film on the surface of the anodic steel, resulting in the early initiation of corrosion (Tennakoon, *et al.*, 2017, Pourbaix, 1996, Shoesmith, *et al.*, 1978). After the initiation of corrosion, the rate of increase of macrocell current was much lower for the AAS concretes compared to the PC concrete (see Fig. 4). This agrees with the results reported by Holloway and Sykes (2005), in which a very low corrosion current was also found for the AAS concretes. Consequently, the charge passed for the AAS concretes was lower than that of PC reference for similar duration of exposure (see Fig. 4). The following reasons are attributed to the above behaviour:

(a) Previous studies (Ma, *et al.*, 2016 and Tennakoon, *et al.*, 2017) reported high bulk resistivity and low chloride diffusivity for AAS concretes. As a result, few chlorides should reach the reinforcing steel in AAS concretes to act as a catalyst to increase further depassivation of the steel. The water soluble and the total chloride concentration at the level of the anodic steel for these ponding slabs were measured at the end of the test (see Table 3). It was noted that the total chloride concentration for the AAS concretes was similar to that for the PC concrete irrespective of slightly longer test durations for the former type. Further, the water soluble chloride concentration was notably low for the AAS concretes. Although water soluble chlorides cannot be equated to free chlorides, it could be interpreted that, for a given test duration, lower amounts of chloride were available for further depassivation of the steel in the AAS concretes. This may explain the reason for the low values of macrocell current measured

in AAS concretes. Further, within the AAS concretes, it seems that the bar in the mix of 6%-1.50 had the lowest charge passed at any given time. From previous study (Ma, *et al.*, 2016) it is known that this mix had the lowest diffusivity. Further, in Table 3 the chloride content at the level of the steel bar is very low for this concrete. Ma *et al.* (2016) reported that this concrete exhibited high bulk resistivity. All of these together contributed to the low charge passed for this concrete.

(b) Glasser (1991) and Andersson *et al.* (1989) reported the redox potential of slag cement is maintained between -150 and -410mV, due to the presence of sulphides, compared to 100 to 200mV for PC (Hewlett, 2003). Redox potential measurement is a reflection of oxidisation and reduction activities. This decreases to a more negative value with the increase of reduction atmosphere. Therefore, the incorporation of slag should make reducing environment of cement stronger and, therefore, protects the embedded steel from oxidisation and lower the rate of corrosion steel. Besides, the oxidation of chemically reduced sulphides would form elemental sulphur to deposit in the pores of the damaged passive film allowing the corroded steel to regain passivation [23]. Similar to slag cement, large amount of sulphides presents in the AAS concretes [5]. Therefore, the steel in such concretes could also regain passivation as a result of the reduction of sulphides and the repair of passivating film. Recently, Mundra *et al.* (2017) confirmed that the presence of sulphides alter the mechanism of corrosion of steel in simulated AAS pore solution. Initiation and pitting were observed to be governed by the pore solution concentration of sulphides and not the chloride concentration as thought for Portland cement systems.

Table 3 also reports the mass loss of the anodic steel bars in the concretes calculated from the macrocell current and compares the results to the one measured gravimetrically.

**Table 3** Total and water soluble chlorides (% by mass of concrete) at the level of the anodic steel after the ponding test and both measured and estimated mass loss of the anodic steel bars

Mix Identify (test duration in days)	Chlorides (% by mass of concrete)		Apparent pH	Mass loss (% of the original mass)		$\frac{\text{Calculated}}{\text{Measured}}\%$
	Total	Water soluble		Measured	Calculated	
4%-0.75 (434)	0.45	0.31	11.35	0.39	0.07	18
4%-1.00 (427)	0.44	0.21	11.40	0.51	0.04	7.8
4%-1.50 (406)	0.45	0.19	11.72	0.50	0.06	12
4%-2.00 (588)	0.54	0.20	11.66	0.38	0.07	18
6%-0.75 (581)	0.40	0.19	11.88	0.29	0.08	28
6%-1.00 (574)	0.34	0.17	11.76	0.21	0.05	24
6%-1.50 (567)	0.28	0.16	12.16	0.26	0.05	19
6%-2.00 (560)	0.34	0.20	11.81	0.33	0.07	21
8%-0.75 (539)	0.45	0.15	12.17	0.29	0.06	21
8%-1.00 (539)	0.46	0.20	11.91	0.27	0.05	18
8%-1.50 (511)	0.45	0.23	12.17	0.34	0.06	18
8%-2.00 (441)	0.44	0.26	11.92	0.63	0.08	13
PC (245)	0.41	0.20	12.61	0.14	0.06	43

### Reliability of $I_{corr}$

From Table 3 it can be seen that the calculated mass loss based on macrocell current was lower than that obtained from the gravimetric measurement. The mass loss based on corrosion current was between 7.8 and 28% of the gravimetric mass loss for AAS concretes. This ratio was 43% for the PC concrete. In the test set-up in Fig. 1, known commonly as the macrocell corrosion test, the expectation is that all of the top bar will act as the anode and all of the bottom bars will act as the cathode. Therefore, by measuring the current between the anode and the cathode, the macrocell corrosion can be determined. However, this set up does not facilitate the measurement of any microcell corrosion between two locations on the top bar (Andrade, et al., 2004). The uneven or non-uniform penetration of chlorides could result in microcell corrosion between an anodic site and an adjacent cathodic site on the same bar, which could be significant, as was observed for all of the AAS concretes in this research. Unfortunately, the current due to microcell corrosion is not easy to measure, despite being significant for all of the AAS concretes. The non-uniform leaching of alkaline material from AAS concretes, resulting in a low pH at different locations of the embedded steel also might have provided a more conductive environment for developing the microcell corrosion in these concretes, as demonstrated by Monticelli *et al.* (2016) for alkali activated class F fly ash mortar specimens.

Fig. 5 shows corrosion of the steel bars in one of the AAS mixes and the PC reference. Due to the different test duration, the extent of corrosion is not comparable between the AAS and PC concretes. In the macrocell set-up, it was intended to make corrosion distributed onto the surface of the entire anodic steel bar (top bar) approximately uniformly. However, as shown in Fig. 5, this is not particularly true for the bar in the AAS concrete. Obvious pitting (anodic region) is observed locally on the surface of the top bar in the AAS concrete, surrounded by larger uncorroded area acting as the cathode, as shown in Fig. 5(a). The pitting corrosion is

considered to be caused by the microcell mentioned above, confirming that microcell corrosion did play a more important role in the corrosion of the steel bars in the AAS concretes. For the bar in PC concrete, the contribution of the macrocell corrosion to the total mass loss was more compared to the AAS concretes (as shown Table 3), which means that a more uniform distribution of corrosion was expected on the surface of the top bar in PC, in which is confirmed by the finding in Fig. 5(b).



(a) AAS - corrosion evident on the highlighted area surrounded by sound regions, localised pitting  
evident



(b) PC - corrosion spread over a larger region

**Fig. 5** Corrosion of the anodic steel bars (top bars) in one of the AAS mix (4%-1.00) and PC reference

Ionic flow through concrete from cathode to anode is required to set up a corrosion cell. The higher electrical resistivity of the AAS concretes (Ma, *et al.*, 2016) and lower diffusivity may have restricted the ionic movement between the electrodes as it does in PC based systems (Dhanya and Santhanam, 2017). This could have favoured the formation of the microcell corrosion in AAS concretes, where anodes and cathodes are formed in the same bar next to each other as compared to macrocell corrosion where anode and cathode are separate bars kept at a distance apart. The distance between the anode and cathode bars must have also played a part in favouring the microcell corrosion. The test set-up in Fig. 1 was adopted from Basheer *et al.* (1998) and is found suitable for PC based systems. In summary, macrocell current measured using this test set-up does not provide a good observation of the corrosion behaviour of AAS concretes. The suitability of macrocell corrosion measurement for PC concrete itself is also questionable given the fact that only 43% of the total corrosion current was due to the macrocell corrosion. This will lead clearly to an underestimation of the corrosion process (Trejo and Monteiro, 2005).

### 3. 2 Half-cell potential

The evolution of half-cell potential of the anodic steel is presented in Fig. 6. This figure also gives the corrosion risk classification using half-cell potential as specified in American Society for Testing Materials C 876 (2009).

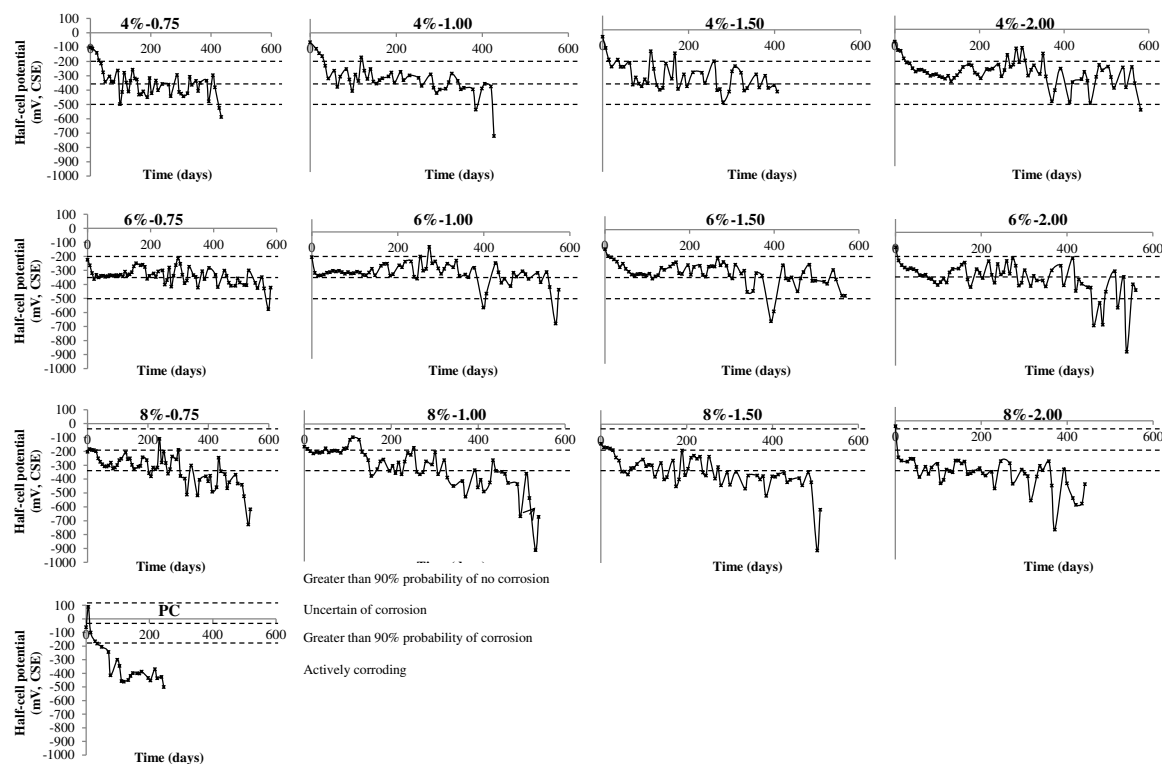


**Fig. 6** Evolution of half-cell potential of the anodic steel bars

Half-cell potentials can be used to characterise the risk of corrosion in PC based concretes. The more negative the value is, the higher is the corrosion risk. According to the guidelines specified in American Society for Testing Materials C 876 (2009), when half-cell potential is more negative than -200mV, steel bar is at a risk of corrosion. Similar to the results reported in (Tennakoon, *et al.*, 2017), a very negative potential value is generally observed for the bars in AAS concretes even at the start of the test. If the ASTM criteria is applied to evaluate these bars, it appears that AAS experience a very severe corrosion. However, the results show that the bars in most of the AAS concretes have a comparable corrosion rate with the bar in PC. As explained by Tennakoon *et al.* (2017), the possible reason for the very negative half-cell potential could be due to the presence of sulphide ions in the pore solution of AAS concretes to reduce the potential values. Consequently, it is questionable to apply the half-cell potential criteria developed for PC concretes for evaluating the corrosion activity of the steel bars in AAS concretes due to such measurement could over-estimate their real corrosion risks.

However, the half-cell potential curves offer similar findings to that of macrocell current results: they are: (a), the anodic steel reacts to the environment early on for AAS concretes; and (b) the rate of reduction of the potential for the AAS concretes was lower compared to the PC reference. This confirms that the corrosion of steel in AAS concretes was initiated at an early stage, while after that, the steel regained passivity to a greater extent. The possible reasons for this have been discussed in the previous section.

#### 4. Conclusions

On the basis of the mixes studied and the tests carried out for the work reported in this paper, the following conclusions have been drawn:

- Corrosion initiates early for AAS concretes despite the low diffusivity and low levels of water soluble chloride concentration. The possible reasons for this observation could be:  
(a) the lower alkalinity of the AAS concretes and (b) the higher concentration of sulphides in the AAS concretes.
- Further to the early initiation, the rate of corrosion based on mass loss measurements is comparable to the PC reference concrete. Several factors could be considered responsible for this phase of corrosion, including the low levels of water soluble chlorides present in the pore solution, the higher bulk resistivity restricting the flow of ions from cathode to anode, and regaining the passivity of the steel due to the reduction reaction in presence of sulphides.
- In a typical macrocell test set-up, microcell corrosion is more likely to occur in the AAS concretes due to their high bulk resistivity. In this work, macrocell current measurements underestimated the extent of corrosion of the steel in the AAS concretes. Only 7.8%-28% of corrosion mass loss was accounted for by the macrocell current for the AAS concretes.
- Conforming to the redox potential values reported for slag based systems, the half-cell potential for AAS concretes remain negative from the start. The rate of decrease of half-cell potential in AAS concretes is much lower than that in PC reference, but it is questionable to apply the half-cell potential criteria developed for PC concretes for evaluating the corrosion risk of the steel in the AAS concretes.

Note that these findings are intended to demonstrate the differential behaviour of AAS mixes compared to Portland systems. However, a detailed investigation to establish the significance

of mix variables and the role played by sulphides is recommended. The authors suggest a factorial experimental design so that both the main and interactive effects of factors could be established for all of the properties measured.

### Acknowledgements

The authors gratefully acknowledge the funding by the EPSRC as part of the UK-China Science Bridge project (EPSRC/G042594/1) and China Scholarship Council. They also acknowledge the support by Queen's University Belfast and University of Leeds for carrying out the experimental work and the EPSRC funding (EP/M003272/1) for the time to prepare and review this article. We also thank Kunming University of Science and Technology for the time allocated to first author for the preparation of this paper. The slag used in this research was supplied by Civil and Marine Ltd.. Dr. Qianmin Ma has been sponsored also by the National Natural Science Foundation of China (NNSFC, Grant Nos.: 52068038, 51502121) and Yunnan Provincial Department of Education (Grant No: 2019J0044). All of these are gratefully acknowledged. The experimental work described in this article was carried out between 2010 and 2013.

### Compliance with ethical standards

### Conflict of interest

The authors declare that they have no conflict of interest.

### List of Notations

PC	Portland cement
AAS	alkali activated slag
GGBS	ground granulated blast furnace slag
Na <sub>2</sub> O%	alkali concentration
Ms	modulus
WG	Sodium silicate solution
W/B	water-binder ratio
$i_{mac}$	macrocell current
$V$	measured electrical potential
$R$	electrical resistance between anodic steel and cathodic steel
$I_{corr}$	corrosion current density
$A$	surface area of the steel bars
$m$	mass loss of the steel
$Q$	charge passed
$M$	molar mass of steel
$F$	Faraday's constant
$z$	valency of Fe
$t$	time

### References

- Al-Otaibi, S. (2008), 'Durability of concrete incorporating GGBS activated by water-glass', *Construction and Building Materials*, Vol. 22, pp. 2059-2067.
- American Society for Testing of Materials, C 876 (2009), *Standard test method for half-cell potentials of uncoated reinforcing steel in concrete*, ASTM International.
- Andersson, K., Allard, B., Bengtsson, M. and Magnusson, B. (1989), 'Chemical composition of cement pore solutions', *Cement and Concrete Research*, Vol. 19(3), pp. 327-332.
- Andrade, C., Alonso, C., Gulikers, J., Polder, R., Cigna, R., Vennesland, O., Salta, M., Raharinaivo, A. and Elsener, B. (2004), RILEM TC 154-EMC: 'Electrochemical techniques for measuring metallic corrosion' Recommendations Test methods for on-site corrosion rate measurement of steel reinforcement in concrete by means of the polarization resistance method, *Materials and Structures*, Vol. 37, pp. 623-643.
- Basheer, L., Cleland, D.J. and Long, A.E. (1998), 'Protection provided by surface treatments against chloride induced corrosion', *Materials and Structures*, Vol. 31, pp. 459-464.

British Standard 1881-125 (1986), *Testing concrete-Part 125: Methods for mixing and sampling fresh concrete in the laboratory*, British Standards Institution.

British Standard EN197-1 (2000), *Cement-Part 1: Composition, specifications and conformity criteria for common cements*, British Standards Institution.

British Standard EN206-1 (2000), *Concrete-Part 1: Specification, performance, production and conformity*, British Standards Institution.

British Standard 8500-1 (2006), *Concrete-complementary British Standard to BS EN 206-1: method of specifying and guidance for the specifier*, British Standards Institution.

British Standard EN 12350-2 (2009), *Testing fresh concrete Part 2:Slump-test*, British Standards Institution.

British Standard EN 12350-3 (2009), *Testing hardened concrete Part 3:Compressive strength of test specimens*, British Standards Institution.

Broomfield, J.P. (2007), *Corrosion of steel in concrete: understanding, investigation and repair*, Taylor & Francis, London.

Criado, M. and Provis, J.L. (2018), ‘Alkali activated slag mortars provide high resistance to chloride-induced corrosion of steel’, *Frontiers of Materials*, 5.34, doi: 10.3389/fmats.2018.00034.

Dhanya, B.S. and Santhanam, M. (2017), ‘Performance evaluation of rapid chloride permeability test in concretes with supplementary cementitious materials’, *Materials and Structures*, Vol. 50 (67).

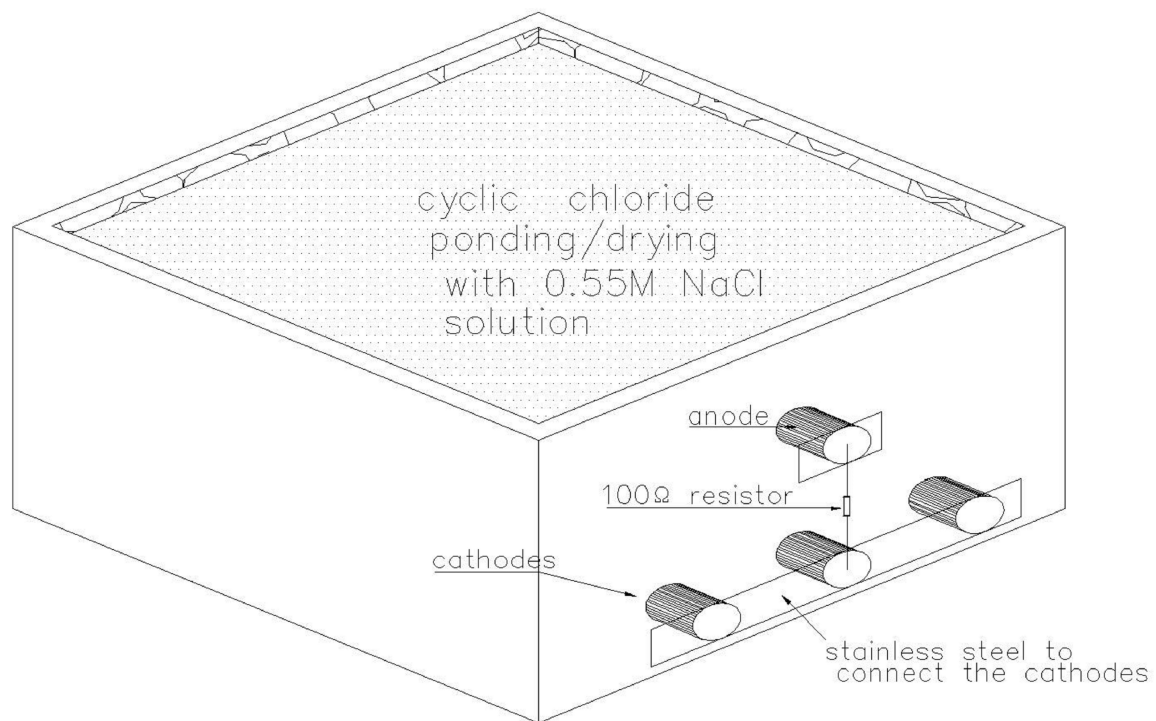
Glasser, F.P. (1991), ‘Chemical, mineralogical, and microstructural changes occurring in hydrated slag-cement blends’, *Material Science of Concrete II*, pp. 41-81.

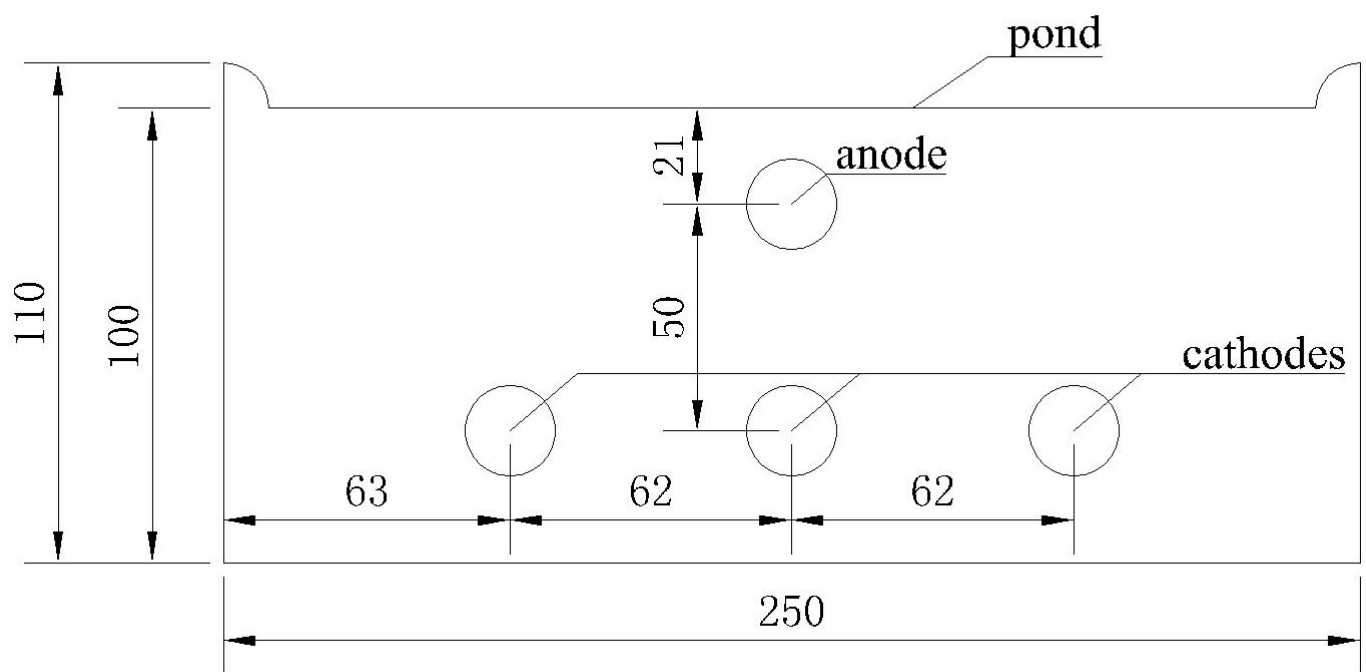
Hewlett, P.C. (2003), *Lea's chemistry of cement and concrete*. Elsevier Science & Technology Books, Amsterdam.

Holloway, M. and Sykes, J.M. (2005), ‘Studies of the corrosion of mild steel in alkali-activated slag cement mortars with sodium chloride admixtures by a galvanostatic pulse method’, *Corrosion Science*, Vol. 47, pp. 3097-3110.

- Johannesson, B., Yamada, K., Nilsson, L-O. and Hosokawa, Y. (2007), 'Multi-species ionic diffusion in concrete with account to interaction between ions in the pore solution and the cement hydrates', *Materials and Structures*, Vol. 40, pp. 51-665.
- Ma, Q., Nanukuttan, S.V., Basheer, P.A.M., Bai, Y. and Yang, C. (2016), 'Chloride transport and the resulting corrosion of steel bars in alkali activated slag concretes', *Materials and Structures*, Vol. 49, pp. 3663-3677.
- Monticelli, C., Natali, M.E., Balbo, A., Chiavari, C., Zanotto, F., Manzi, S. and Bignozzi, M.C. (2016), 'A study of the corrosion of reinforcing bars in alkali-activated fly ash mortars under wet and dry exposures to chloride solutions', *Cement and Concrete Research*, Vol. 87, pp. 53-63.
- Mundra, S., Bernal, S. and Provis, J. (2017), 'Corrosion initiation of steel reinforcement in simulated alkali-activated slag pore solutions', 1<sup>st</sup> International Conference on Construction Materials for Sustainable Future, 19-21 April 2017, Zadar, Croatia.
- Pourbaix, M. (1966), *Atlas of electrochemical equilibria in aqueous solutions*, Pergamon Press, Oxford.
- Ravikumar, D. and Neithalath, N. (2013), 'Electrically induced chloride ion transport in alkali activated slag concretes and the influence of microstructure', *Cement and Concrete Research*, Vol. 47, pp. 31-42.
- RILEM TC 178-TMC (2002a), 'Testing and modelling chloride penetration in concrete' analysis of total chloride content in concrete recommendation', *Materials and Structures*, Vol. 35, pp. 583-585.
- RILEM TC 178-TMC (2002b), 'Testing and modelling chloride penetration in concrete' Analysis of water soluble chloride content in concrete recommendation', *Materials and Structures*, Vol. 35, pp. 586-588.
- Runci, A. and Serdar, M. (2020), 'Chloride-induced corrosion of steel in alkali-activated mortars based on different precursors', *Materials*, Vol. 13(22), doi:10.3390/ma13225244.
- Shi, C., Krivenko, P.V. and Roy, D. (2006), *Alkali-Activated Cements and Concretes*, Taylor & Francis, London.

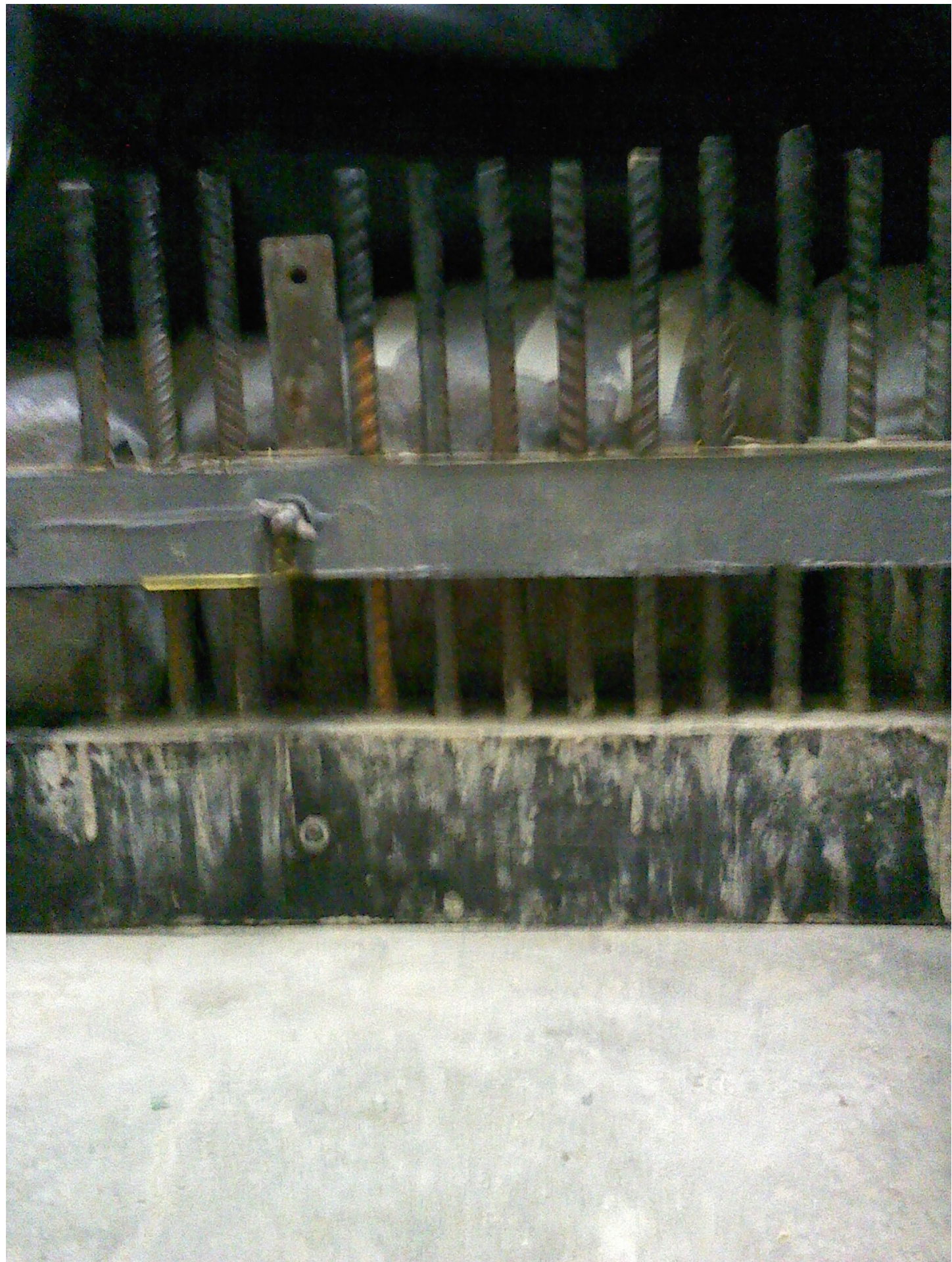
- Shoesmith, D.W., Taylor, P., Bailey, M.G. and Ikeda, B. (1978), 'Electrochemical behaviour of iron in alkaline sulphide solutions', *Electrochimica Acta*, Vol. 23, pp. 903-916.
- Tennakoon, C., Shayan, A., Sanjayan, J.G. and Xu, A. (2017), 'Chloride ingress and steel corrosion in geopolymer concrete based on long term tests', *Materials and Design*, Vol. 116, pp. 287-299.
- Torres-Carrasco, M., Tognonvi, M.T., Taguit-Hamou, A. and Puertas, F (2015), 'Durability of alkali-activated slag concretes prepared using waste glass as alternative activator'. *ACI Materials Journal*, Vol. 112, pp. 791-800.
- Trejo, D. and Monteiro, P.J. (2005), 'Corrosion performance of conventional (ASTM A615) and low-alloy (ASTM A706) reinforcing bars embedded in concrete and exposed to chloride environments', *Cement and Concrete Research*, Vol. 35, pp. 562-571.
- Yang, C. and Pu, X. (1993), 'Retarder of alkali activated slag', *Chinese patent 91108316.2*.
- You, N., Shi, J. and Zhang, Y. (2020), 'Corrosion behaviour of low-carbon steel reinforcement in alkali-activated slag-steel slag and Portland cement-based mortars under simulated marine environment', *Corrosion Science*, Vol. 175, Article No. 108874.





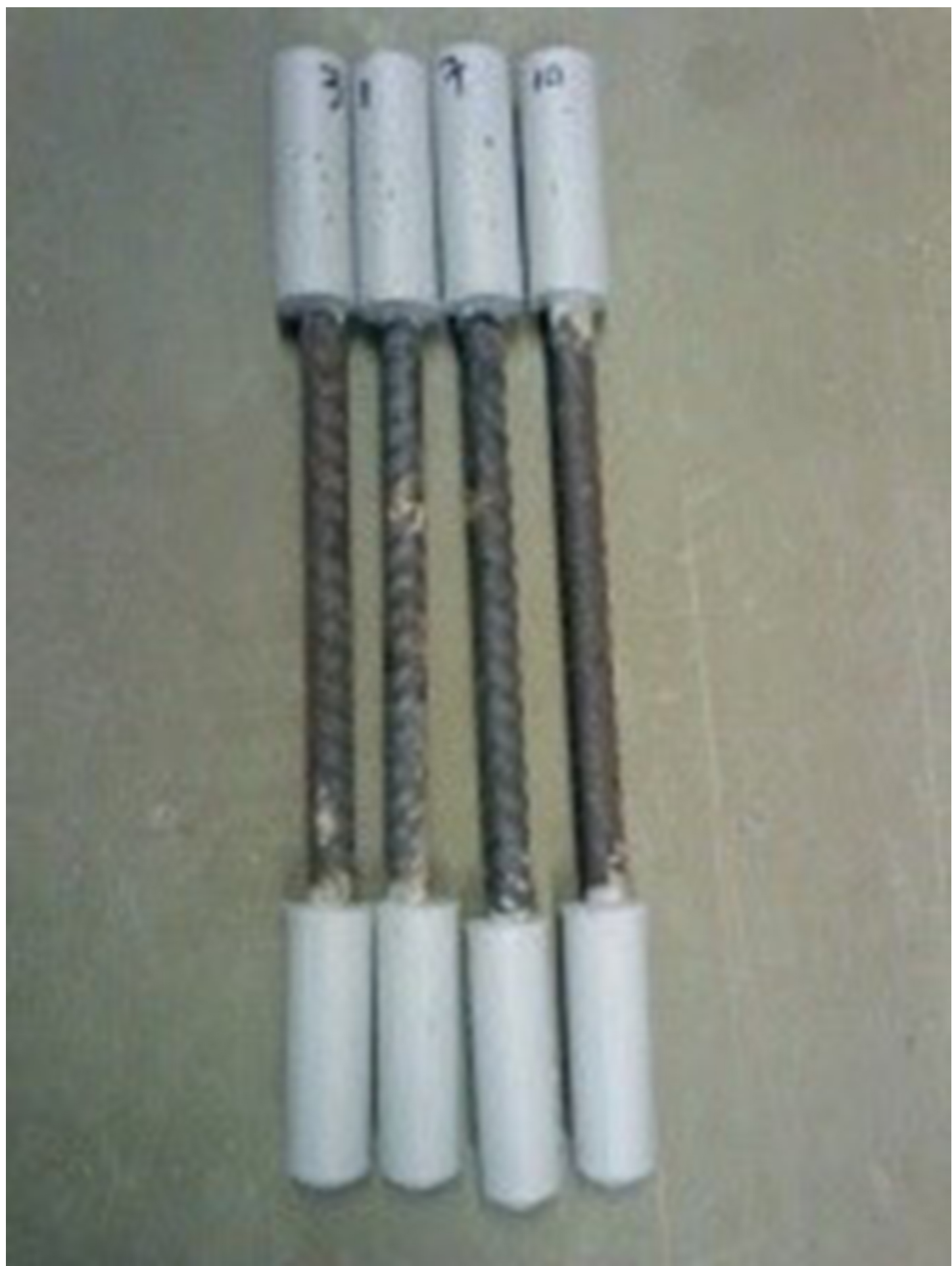






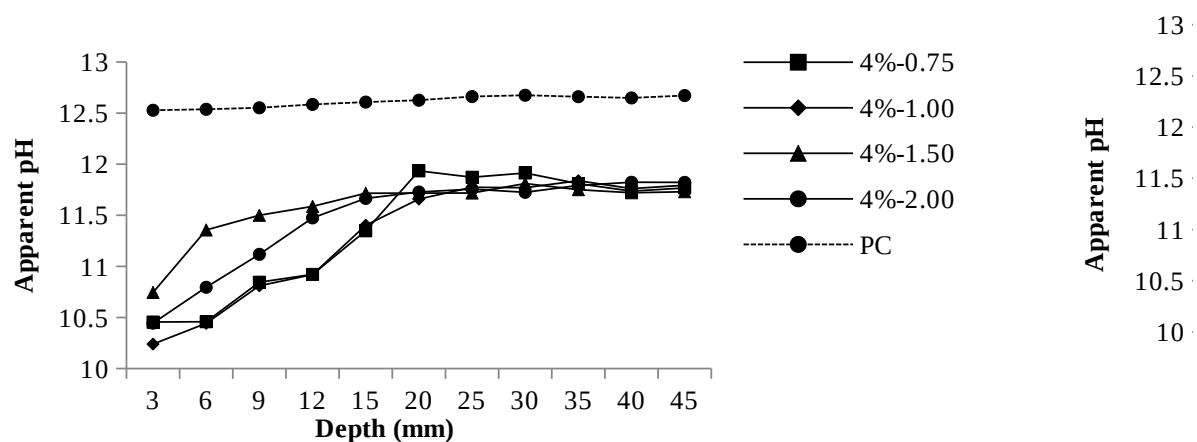




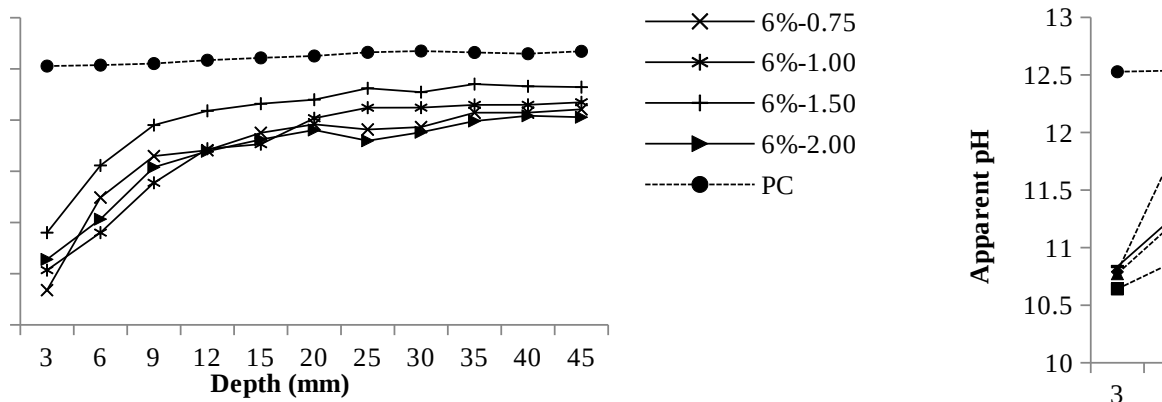


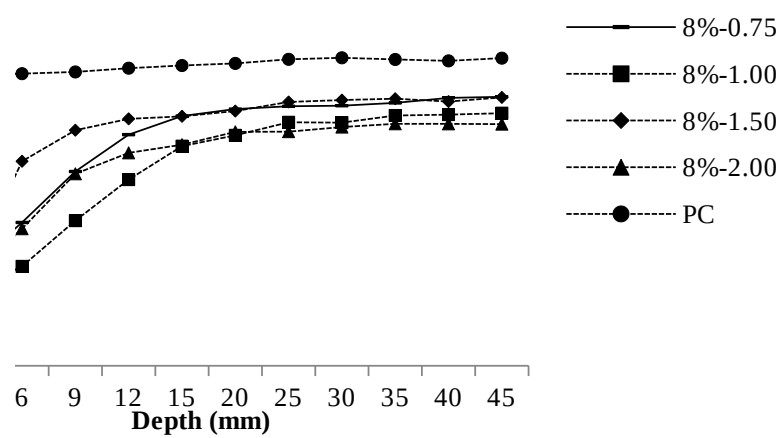


	PC	4%-0.75	4%-1.00	4%-1.50	4%-2.00	6%-0.75	6%-1.00
3	12.527667	10.45531	10.239333	10.744519	10.444333	10.33946	10.53467
6	12.537	10.458039	10.442667	11.355839	10.795333	11.24375	10.901
9	12.552	10.845182	10.810333	11.499653	11.117667	11.64821	11.38733
12	12.584667	10.92158	10.919333	11.586397	11.474	11.70533	11.72
15	12.607667	11.347832	11.401667	11.715144	11.664667	11.87568	11.76433
20	12.626	11.934157	11.658333	11.716514	11.727333	11.95831	12.01767
25	12.661667	11.871705	11.773333	11.717427	11.755667	11.90782	12.12033
30	12.674667	11.913542	11.769333	11.810107	11.724333	11.93153	12.12133
35	12.660333	11.809202	11.837667		11.75	11.791667	12.07207
40	12.648	11.735728	11.760667		11.72	11.822667	12.07265
45	12.671667	11.766899	11.793333		11.73	11.821667	12.10457

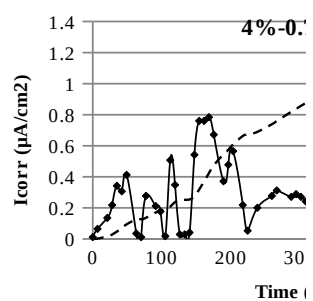


6%-1.50	6%-2.00	8%-0.75	8%-1.00	8%-1.50	8%-2.00
10.901	10.63967	10.83567	10.641	10.79	10.77367
11.557	11.03267	11.24467	10.86367	11.77567	11.19
11.951	11.53933	11.68733	11.26033	12.04567	11.667
12.09	11.695	12.007	11.617	12.14433	11.849
12.159	11.80967	12.16867	11.907	12.166	11.92
12.199	11.90267	12.229	12.00133	12.212	12.03167
12.311	11.79767	12.25367	12.11433	12.291	12.033
12.273	11.88067	12.25833	12.11167	12.30733	12.073
12.352	11.99033	12.283	12.17333	12.31933	12.10133
12.33	12.04167	12.32667	12.18133	12.29467	12.10067
12.322	12.028	12.336	12.19367	12.33067	12.09867

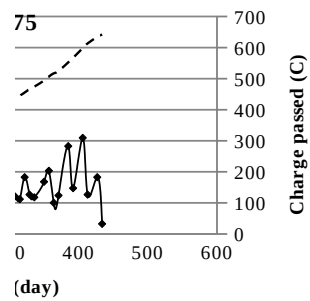




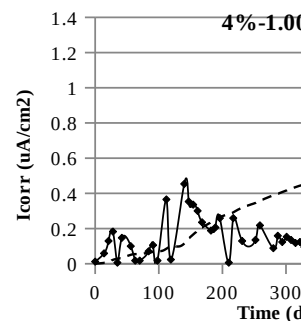
Time (day)	Icorr ( $\mu\text{A}/\text{cm}^2$ )	charge passed/C
0	0.0117889773062	0
7	0.0648393751842	1.3104
21	0.1355732390215	8.1648
28	0.218096080165	14.2128
35	0.3418803418803	23.7888
42	0.3065134099617	34.8768
49	0.4126142057177	47.1744
63	0.0353669319187	62.496
70	0.0117889773062	63.3024
77	0.2770409666961	68.2416
91	0.2122015915119	84.9744
98	0.1768346595933	91.6272
105	0.0176834659593	94.9536
112	0.5069260241674	103.9248
119	0.3477748305335	118.5408
126	0.0294724432655	124.992
133	0.0294724432655	126
140	0.0412614205718	127.2096
147	0.5422929560861	137.1888
154	0.7603890362511	159.4656
161	0.7603890362511	185.472
168	0.7839669908635	211.8816
175	0.6719717064545	236.7792
182		
189	0.3713527851459	272.4624
196	0.4774535809019	286.9776
203	0.5658709106985	304.8192
210		
217	0.218096080165	331.632
224	0.053050397878	336.2688
231		
238	0.2004126142057	344.9376
245		
252		
259	0.2770409666961	369.432
266	0.3124078986148	379.512
273		
280		
287	0.271146478043	409.4496
294	0.2888299440024	419.0256
301	0.271146478043	428.6016
308	0.2416740347775	437.3712
315	0.2239905688182	445.3344
322	0.3654582964928	455.4144
329	0.2534630120837	465.9984
336	0.2357795461244	474.3648
343		
350	0.3359858532272	493.92
357	0.4067197170645	506.6208
364	0.2004126142057	517.0032
371	0.2475685234306	524.664
378		
385	0.5658709106985	552.4848



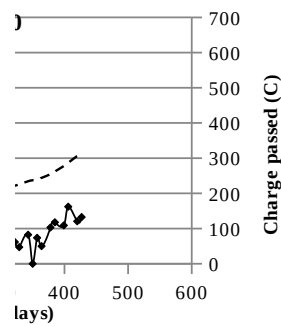
392	0.2947244326555	567.2016
399		
406	0.6189213085765	598.4496
413	0.2534630120837	613.368
420		
427	0.3654582964928	634.536
434	0.0648393751842	641.8944



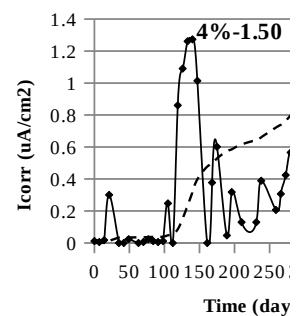
Time (day)	Icorr ( $\mu\text{A}/\text{cm}^2$ )	charge passed/C
0	0.01178897730622	0
7		
14	0.05894488653109	2.4192
21	0.12967875036841	5.6448
28	0.18272914824639	10.9872
35	0.00589448865311	14.2128
42	0.14736221632773	16.8336
56	0.10020630710286	25.3008
63	0.01768346595933	27.3168
70	0.01768346595933	27.9216
84	0.07073386383731	30.9456
91	0.10610079575597	33.9696
98	0.01768346595933	36.0864
105		36.3888
112	0.36545829649278	42.6384
119	0.02357795461244	49.2912
126		49.6944
133		49.6944
140	0.45387562628942	57.456
147	0.35366931918656	71.2656
154	0.33598585322723	83.0592
161	0.30061892130858	93.9456
168	0.23577954612437	103.1184
175		
182	0.1886236368995	117.6336
189	0.20630710285883	124.3872
196	0.25935750073681	132.3504
203		
210	0.00589448865311	141.4224
217	0.25935750073681	145.9584
224		
231	0.12967875036841	159.264
238		
245		
252	0.13557323902152	172.872
259	0.21809608016505	178.92
266		
273		
280	0.08841732979664	194.6448
287	0.15915119363395	198.8784
294	0.1237842617153	203.7168
301	0.15325670498084	208.4544
308	0.13557323902152	213.3936
315	0.11788977306219	217.728
322	0.1237842617153	221.8608
329	0.09431181844975	225.5904
336		
343	0.16504568228706	234.4608
350	0	237.2832
357	0.14736221632773	239.8032
364	0.10020630710286	244.0368
371		
378	0.20630710285883	254.52



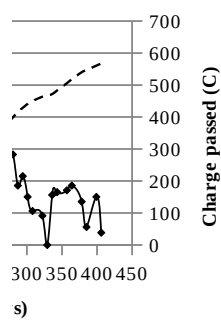
385	0.23577954612437	262.08
392		
399	0.21809608016505	277.6032
406	0.32419687592101	286.8768
413		
420	0.24167403477748	306.2304
427	0.26525198938992	314.8992



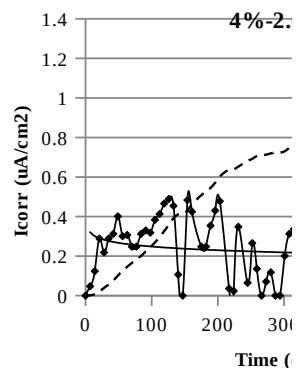
Time (day)	Icorr (uA/cm <sup>2</sup> )	charge passed/C
0	0.0117889773062	0
7	0.0058944886531	0.3024
14	0.0176834659593	0.7056
21	0.3006189213086	6.1488
35	0	16.4304
42	0	16.4304
49	0.0235779546124	16.8336
63	0	17.64
70	0.0058944886531	17.7408
77	0.0235779546124	18.2448
84	0.0117889773062	18.8496
91	0.0058944886531	19.152
98	0.0117889773062	19.4544
105	0.2475685234306	23.8896
112	0	28.1232
119	0.860595343354	42.84
126	1.0904804008252	76.2048
133	1.2614205717654	116.424
140	1.2732095490716	159.768
147	1.0138520483348	198.8784
154		
161	0	238.5936
168	0.377247273799	247.5648
175	0.6012378426172	264.2976
182		
189	0.0471559092249	286.4736
196	0.3183023872679	292.7232
203		
210	0.1296787503684	308.0448
217		
224		
231	0.1296787503684	321.3504
238	0.3890362511052	330.2208
245		
252		
259	0.2063071028588	360.7632
266	0.3065134099617	369.5328
273	0.4244031830239	382.032
280	0.5658709106985	398.9664
287	0.3713527851459	414.9936
294	0.430297671677	428.7024
301	0.3006189213086	441.2016
308	0.2122015915119	449.9712
315		
322	0.1827291482464	463.4784
329	0	466.6032
336	0.3124078986148	471.9456
343	0.3300913645741	482.9328
350		
357	0.3418803418803	505.9152
364	0.3713527851459	518.112
371		
378	0.271146478043	540.0864



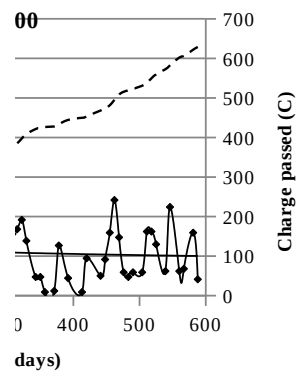
385	0.1119952844091	546.6384
392		
399	0.3006189213086	560.7504
406	0.0766283524904	567.2016



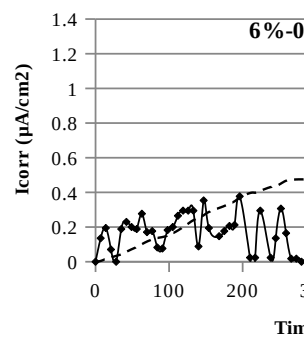
Time (day)	Icorr ( $\mu\text{A}/\text{cm}^2$ )	charge passed/C
0	0	0
7	0.0471559092249	0.8064
14	0.1237842617153	3.7296
21	0.2888299440024	10.7856
28	0.218096080165	19.4544
35	0.2888299440024	28.1232
42	0.3124078986148	38.4048
49	0.4008252284114	50.6016
56	0.3006189213086	62.5968
63	0.3065134099617	72.9792
70	0.2475685234306	82.4544
77	0.2475685234306	90.9216
84	0.3124078986148	100.4976
91	0.3300913645741	111.4848
98	0.3183023872679	122.5728
105	0.3831417624521	134.568
112	0.4126142057177	148.176
119	0.4656646035956	163.1952
126	0.4892425582081	179.5248
133	0.4538756262894	195.6528
140	0.106100795756	205.2288
147	0	207.0432
154	0.483348069555	215.3088
161	0.4244031830239	230.832
175	0.2475685234306	253.8144
182	0.2475685234306	262.2816
189	0.3536693191866	272.5632
196	0.430297671677	285.9696
203	0.4774535809019	301.4928
217	0.0353669319187	319.032
224	0.0235779546124	320.04
231	0.3477748305335	326.3904
245	0.0648393751842	340.5024
252	0.2652519893899	346.1472
259	0.1355732390215	353.0016
266	0	355.32
273	0.0707338638373	356.5296
280	0.1178897730622	359.7552
287	0	361.7712
294	0	361.7712
301	0.2004126142057	365.1984
308	0.3124078986148	373.968
315	0.3359858532272	385.056
322	0.3831417624521	397.3536
329	0.2770409666961	408.6432
336		
343	0.0943118184497	421.344
350	0.0943118184497	424.5696
357	0.0176834659593	426.4848
364		
371	0.0235779546124	427.896
378	0.2534630120837	432.6336
385		



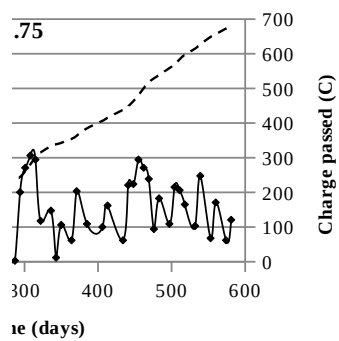
392	0.0884173297966	444.3264
399		
406		
413	0.0176834659593	449.7696
420	0.1886236368995	453.2976
427		
434		
441	0.1002063071029	468.1152
448	0.1827291482464	472.9536
455	0.3183023872679	481.5216
462	0.483348069555	495.2304
469	0.2947244326555	508.536
476	0.1178897730622	515.592
483	0.0943118184497	519.2208
490	0.1178897730622	522.8496
497		
504	0.1178897730622	530.9136
511	0.324196875921	538.4736
518	0.324196875921	549.5616
525	0.2593575007368	559.5408
532		
539	0.1237842617153	572.6448
546	0.4479811376363	582.4224
553		
560	0.1237842617153	601.9776
567	0.1355732390215	606.4128
574		
581	0.3183023872679	621.936
588	0.0825228411435	628.7904



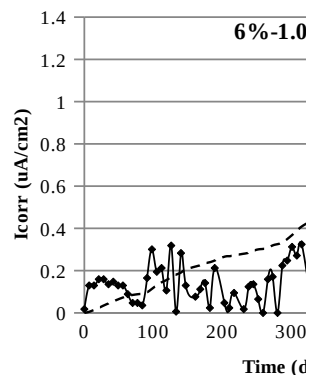
Time (day)	Icorr ( $\mu\text{A}/\text{cm}^2$ )	charge passed/C
0	0	0
7	0.1355732390215	2.3184
14	0.1945181255526	7.9632
21	0.0707338638373	12.4992
28	0	
35	0.1886236368995	21.3696
42	0.2298850574713	28.5264
49	0.2004126142057	35.8848
56	0.1886236368995	42.5376
63	0.2770409666961	50.5008
70	0.1709401709402	58.1616
77	0.1768346595933	64.1088
84	0.0825228411435	68.544
91	0.0766283524904	71.2656
98	0.1827291482464	75.7008
105	0.2004126142057	82.2528
112	0.2652519893899	90.216
119	0.2947244326555	99.792
126	0.2947244326555	109.872
133	0.2947244326555	119.952
140	0.0884173297966	126.504
147	0.3536693191866	134.064
154	0.1945181255526	143.4384
168	0.1473622163277	155.1312
175	0.1768346595933	160.6752
182	0.2063071028588	167.2272
189	0.2122015915119	174.384
196	0.377247273799	184.464
210	0.0235779546124	198.1728
217	0.0235779546124	198.9792
224	0.2947244326555	204.4224
238	0.0235779546124	215.3088
245	0.1355732390215	218.0304
252	0.3065134099617	225.5904
259	0.1650456822871	233.6544
266	0.0176834659593	236.7792
273	0.0176834659593	237.384
280	0	237.6864
287	0.0058944886531	237.7872
294	0.4008252284114	244.7424
301	0.5422929560861	260.8704
308	0.6130268199234	280.6272
315	0.5894488653109	301.1904
322	0.2357795461244	315.3024
329		
336	0.2947244326555	333.4464
343	0.0235779546124	338.8896
350	0.2122015915119	342.9216
357		
364	0.1237842617153	354.4128
371	0.4067197170645	363.4848
378		
385	0.218096080165	384.8544



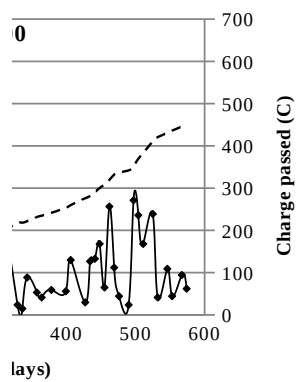
392		
399		
406	0.2004126142057	406.3248
413	0.324196875921	415.296
420		
427		
434	0.1237842617153	438.2784
441	0.4420866489832	447.9552
448	0.4479811376363	463.176
455	0.5894488653109	480.9168
462	0.5422929560861	500.2704
469	0.4774535809019	517.7088
476	0.1886236368995	529.0992
483	0.3654582964928	538.5744
490		
497	0.218096080165	558.5328
504	0.430297671677	569.6208
511	0.4126142057177	584.0352
518	0.3300913645741	596.736
525		
532	0.2063071028588	615.0816
539	0.4951370468612	627.0768
546		
553	0.1355732390215	648.648
560	0.3418803418803	656.8128
567		
574	0.1237842617153	672.7392
581	0.2416740347775	678.9888



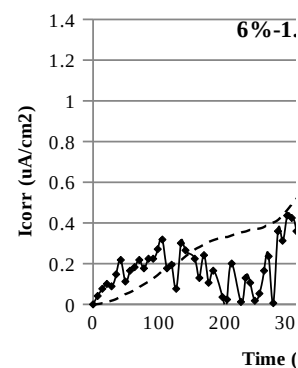
Time (day)	Icorr ( $\mu\text{A}/\text{cm}^2$ )	charge passed/C
0	0.0176834659593	0
7	0.1296787503684	2.52
14	0.1296787503684	6.9552
21	0.159151193634	11.8944
28	0.159151193634	17.3376
35	0.1355732390215	22.3776
42	0.1473622163277	27.216
49	0.1296787503684	31.9536
56	0.1296787503684	36.3888
63	0.0884173297966	40.1184
70	0.0471559092249	42.4368
77	0.0471559092249	44.0496
84	0.0353669319187	45.4608
91	0.1650456822871	48.888
98	0.3006189213086	56.8512
105	0.1945181255526	65.3184
112	0.2122015915119	72.2736
119	0.106100795756	77.7168
126	0.3183023872679	84.9744
133	0.0058944886531	90.5184
140	0.2829354553492	95.4576
147	0.1296787503684	102.5136
161	0.0766283524904	109.5696
168	0.1119952844091	112.7952
175	0.1414677276746	117.1296
182	0.0235779546124	119.952
189	0.2122015915119	123.984
203	0.0471559092249	132.8544
210	0.0235779546124	134.064
217	0.0943118184497	136.08
231	0.0176834659593	139.9104
238	0.1237842617153	142.3296
245	0.1355732390215	146.7648
252	0.0648393751842	150.192
259	0	151.3008
266	0.159151193634	154.0224
273	0.1709401709402	159.6672
280	0	162.5904
287	0.2239905688182	166.4208
294	0.2475685234306	174.4848
301	0.3124078986148	184.0608
308	0.271146478043	194.04
315	0.324196875921	204.2208
322		
329	0.0471559092249	216.9216
336	0.0294724432655	218.232
343	0.1768346595933	221.76
350		
357	0.106100795756	231.4368
364	0.0825228411435	234.6624
371		
378	0.1178897730622	241.5168
385		



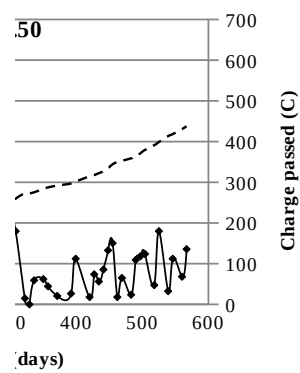
392		
399	0.1119952844091	253.3104
406	0.2593575007368	259.6608
413		
420		
427	0.0589448865311	275.9904
434	0.2534630120837	281.3328
441	0.2652519893899	290.2032
448	0.3359858532272	300.4848
455	0.1296787503684	308.448
462	0.5128205128205	319.4352
469	0.2239905688182	332.0352
476	0.0884173297966	337.3776
483		
490	0.0471559092249	342.0144
497	0.5422929560861	352.0944
504	0.4715590922487	369.432
511	0.3359858532272	383.2416
518		
525	0.4774535809019	411.0624
532	0.0825228411435	420.6384
539		
546	0.218096080165	430.92
553	0.0884173297966	436.1616
560		
567	0.1886236368995	445.6368
574	0.1237842617153	450.9792



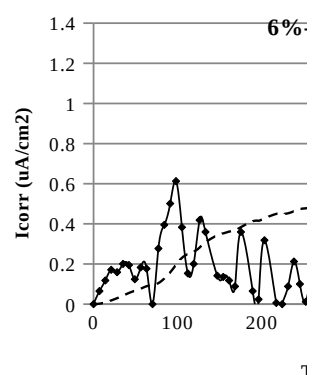
Time (day)	Icorr ( $\mu\text{A}/\text{cm}^2$ )	charge passed/C
0	0	0
7	0.0412614205718	0.7056
14	0.0766283524904	2.7216
21	0.1002063071029	5.7456
28	0.0884173297966	8.9712
35	0.1473622163277	13.0032
42	0.218096080165	19.2528
49	0.1119952844091	24.8976
56	0.1650456822871	29.6352
63	0.1827291482464	35.5824
70	0.218096080165	42.4368
77	0.1768346595933	49.1904
84	0.2239905688182	56.0448
91	0.2239905688182	63.7056
98	0.271146478043	72.1728
105	0.3183023872679	82.2528
112	0.1768346595933	90.72
119	0.1945181255526	97.0704
126	0.0766283524904	101.7072
133	0.3006189213086	108.1584
140	0.2652519893899	117.8352
154	0.2239905688182	134.568
161	0.1296787503684	140.616
168	0.2416740347775	146.9664
175	0.106100795756	152.9136
182	0.1650456822871	157.5504
196	0.0353669319187	164.4048
203	0.0235779546124	165.4128
210	0.2004126142057	169.2432
224	0.0117889773062	176.5008
231	0.1296787503684	178.92
238	0.106100795756	182.952
245	0.0176834659593	185.0688
252	0.053050397878	186.2784
259	0.1650456822871	190.008
266	0.2357795461244	196.8624
273	0.0058944886531	200.9952
280	0.3595638078397	207.2448
287	0.3124078986148	218.736
294	0.4361921603301	231.5376
301	0.4244031830239	246.2544
308	0.3595638078397	259.6608
315		
322	0.0294724432655	272.9664
329	0	273.4704
336	0.1178897730622	275.4864
343		
350	0.1237842617153	283.752
357	0.0884173297966	287.3808
364		
371	0.0412614205718	291.816
378		
385		



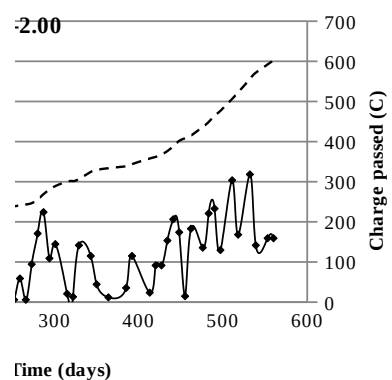
392	0.053050397878	296.6544
399	0.2239905688182	301.392
406		
413		
420	0.0353669319187	314.6976
427	0.1473622163277	317.8224
434	0.1119952844091	322.2576
441	0.1709401709402	327.096
448	0.2652519893899	334.5552
455	0.3006189213086	344.232
462	0.0353669319187	349.9776
469	0.1296787503684	352.8
476		
483	0.0471559092249	358.848
490	0.218096080165	363.384
497	0.2357795461244	371.1456
504	0.2475685234306	379.4112
511		
518	0.0943118184497	391.104
525	0.3595638078397	398.8656
532		
539	0.0648393751842	413.3808
546	0.2239905688182	418.32
553		
560	0.1355732390215	430.6176
567	0.271146478043	437.5728



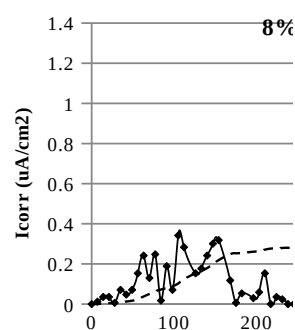
Time (day)	Icorr (uA/cm <sup>2</sup> )	charge passed/C
0	0	0
7	0.0648393751842	1.1088
14	0.1178897730622	4.2336
21	0.1709401709402	9.1728
28	0.159151193634	14.8176
35	0.2004126142057	20.9664
42	0.1945181255526	27.72
49	0.1237842617153	33.1632
56	0.1827291482464	38.4048
63	0.1768346595933	44.5536
70	0	47.5776
77	0.2770409666961	52.3152
84	0.3949307397583	63.8064
91	0.5010315355143	79.128
98	0.6130268199234	98.1792
105	0.3831417624521	115.2144
112	0.1532567049808	124.3872
119	0.2004126142057	130.4352
126	0.4185086943708	141.0192
133	0.3595638078397	154.3248
147	0.1414677276746	171.4608
154	0.1355732390215	176.1984
161	0.1178897730622	180.5328
168	0.0884173297966	184.0608
175	0.3595638078397	191.7216
189	0.0648393751842	206.2368
196	0.0235779546124	207.7488
203	0.3183023872679	213.5952
217	0.0058944886531	224.6832
224	0	224.784
231	0.0884173297966	226.296
238	0.2122015915119	231.4368
245	0.1002063071029	236.7792
252	0.0117889773062	238.6944
259	0.1178897730622	240.912
266	0.0117889773062	243.1296
273	0.1886236368995	246.5568
280	0.3418803418803	255.6288
287	0.4479811376363	269.136
294	0.218096080165	280.5264
301	0.2888299440024	289.1952
308		
315	0.0412614205718	300.4848
322	0.026525198939	301.644
329	0.2829354553492	306.936
336		
343	0.2298850574713	324.4752
350	0.0884173297966	329.9184
357		
364	0.0235779546124	333.7488
371		
378		
385	0.0707338638373	338.5872



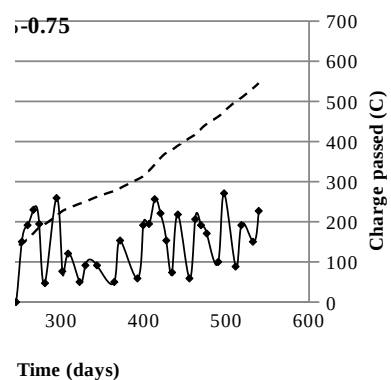
392	0.2298850574713	343.728
399		
406		
413	0.0471559092249	357.9408
420	0.1827291482464	361.872
427	0.1827291482464	368.1216
434	0.3065134099617	376.488
441	0.4126142057177	388.7856
448	0.3477748305335	401.7888
455	0.0294724432655	408.24
462	0.3654582964928	414.9936
469		
476	0.271146478043	436.7664
483	0.4420866489832	448.9632
490	0.4656646035956	464.4864
497	0.2593575007368	476.8848
504		
511	0.6071323312703	506.52
518	0.3359858532272	522.648
525		
532	0.6366047745358	555.912
539	0.2829354553492	571.6368
546		
553	0.3183023872679	592.2
560	0.3183023872679	603.0864



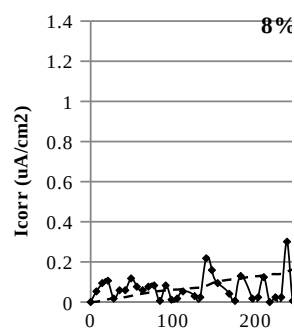
Time (day)	Icorr ( $\mu\text{A}/\text{cm}^2$ )	charge passed/C
0	0	0
7	0.0117889773062	0.2016
14	0.0353669319187	1.008
21	0.0353669319187	2.2176
28	0.0058944886531	2.9232
35	0.0707338638373	4.2336
42	0.0471559092249	6.2496
49	0.0707338638373	8.2656
56	0.1532567049808	12.096
63	0.2416740347775	18.8496
70	0.1296787503684	25.2
77	0.2475685234306	31.6512
84	0.0176834659593	36.1872
91	0.1886236368995	39.7152
98	0.0707338638373	44.1504
105	0.3418803418803	51.2064
112	0.2829354553492	61.8912
126	0.1532567049808	76.8096
133	0.1768346595933	82.4544
140	0.2416740347775	89.6112
147	0.3006189213086	98.8848
154	0.3183023872679	109.4688
168	0.1178897730622	124.3872
175	0.0058944886531	126.504
182	0.053050397878	127.512
196	0.0294724432655	130.3344
203	0.0589448865311	131.8464
210	0.1532567049808	135.4752
217	0	138.096
224	0.0353669319187	138.7008
231	0.0235779546124	139.7088
238	0	140.112
245	0	140.112
252	0.3006189213086	145.2528
259	0.3831417624521	156.9456
266	0.4597701149425	171.36
273	0.3890362511052	185.8752
280	0.0943118184497	194.1408
287		
294	0.5187150014736	215.1072
301	0.1532567049808	226.5984
308	0.2416740347775	233.352
315		
322	0.1002063071029	245.0448
329	0.1827291482464	249.8832
336		
343	0.1827291482464	262.3824
350		
357		
364	0.1002063071029	276.8976
371	0.3065134099617	283.8528
378		
385		



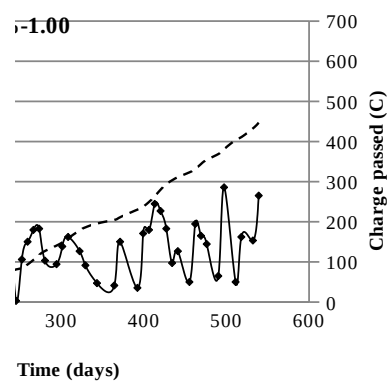
392	0.1178897730622	305.6256
399	0.3831417624521	314.1936
406	0.3890362511052	327.3984
413	0.5128205128205	342.8208
420	0.4420866489832	359.1504
427	0.3065134099617	371.952
434	0.1473622163277	379.7136
441	0.4361921603301	389.6928
448		
455	0.1178897730622	408.6432
462	0.4126142057177	417.7152
469	0.3831417624521	431.3232
476	0.3418803418803	443.7216
483		
490	0.2004126142057	462.2688
497	0.5422929560861	474.9696
504		
511	0.1768346595933	499.5648
518	0.3831417624521	509.1408
525		
532	0.3006189213086	532.5264
539	0.4538756262894	545.4288



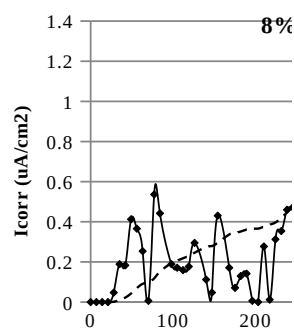
Time (day)	Icorr ( $\mu\text{A}/\text{cm}^2$ )	charge passed/C
0	0	0
7	0.053050397878	0.9072
14	0.0943118184497	3.4272
21	0.106100795756	6.8544
28	0.0176834659593	8.9712
35	0.0589448865311	10.2816
42	0.0589448865311	12.2976
49	0.1178897730622	15.3216
56	0.0766283524904	18.648
63	0.0589448865311	20.9664
70	0.0766283524904	23.2848
77	0.0825228411435	26.0064
84	0.0058944886531	27.5184
91	0.0825228411435	29.0304
98	0.0117889773062	30.6432
105	0.0176834659593	31.1472
112	0.053050397878	32.3568
126	0.0294724432655	35.1792
133	0.0235779546124	36.0864
140	0.218096080165	40.2192
147	0.159151193634	46.6704
154	0.0943118184497	51.0048
168	0.0412614205718	55.6416
175	0.0058944886531	56.448
182	0.1296787503684	58.7664
196	0.0176834659593	63.8064
203	0.0235779546124	64.512
210	0.1237842617153	67.032
217	0	69.1488
224	0.0235779546124	69.552
231	0.0235779546124	70.3584
238	0.3006189213086	75.9024
245	0.0058944886531	81.144
252	0.2122015915119	84.8736
259	0.3006189213086	93.6432
266	0.3595638078397	104.9328
273	0.3654582964928	117.3312
280	0.2063071028588	127.1088
287		
294	0.1886236368995	140.616
301	0.2770409666961	148.5792
308	0.324196875921	158.8608
315		
322	0.2534630120837	178.6176
329	0.1827291482464	186.0768
336		
343	0.0943118184497	195.552
350		
357		
364	0.0825228411435	204.624
371	0.3006189213086	211.176
378		
385		



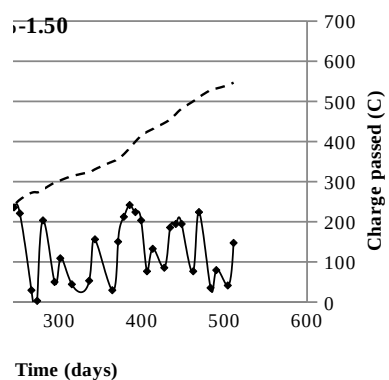
392	0.0707338638373	230.2272
399	0.3418803418803	237.2832
406	0.3595638078397	249.2784
413	0.4892425582081	263.7936
420	0.4538756262894	279.9216
427	0.3654582964928	293.9328
434	0.1945181255526	303.5088
441	0.2534630120837	311.1696
448		
455	0.1002063071029	323.2656
462	0.3890362511052	331.632
469	0.3300913645741	343.9296
476	0.2888299440024	354.5136
483		
490	0.1296787503684	368.8272
497	0.5717653993516	380.8224
504		
511	0.1002063071029	403.8048
518	0.324196875921	411.0624
525		
532	0.3065134099617	432.6336
539	0.5305039787798	446.9472



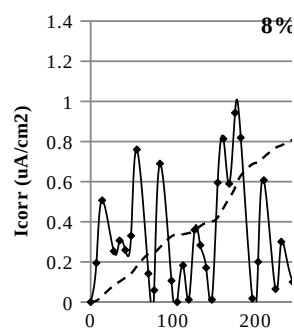
Time (day)	Icorr ( $\mu\text{A}/\text{cm}^2$ )	charge passed/C
0	0	0
7	0	0
14	0	0
21	0	0
28	0.0471559092249	0.8064
35	0.1886236368995	4.8384
42	0.1827291482464	11.1888
49	0.4126142057177	21.3696
56	0.3654582964928	34.6752
63	0.2534630120837	45.2592
70	0.0058944886531	49.6944
77	0.536398467433	58.968
84	0.4420866489832	75.7008
98	0.1886236368995	97.272
105	0.1709401709402	103.4208
112	0.159151193634	109.0656
119	0.1768346595933	114.8112
126	0.2947244326555	122.8752
140	0.1119952844091	136.7856
147	0.0471559092249	139.5072
154	0.430297671677	147.672
168	0.1709401709402	168.2352
175	0.0707338638373	172.368
182	0.1296787503684	175.7952
189	0.1414677276746	180.432
196	0.0058944886531	182.952
203	0	183.0528
210	0.2770409666961	187.7904
217	0.0117889773062	192.7296
224	0.3124078986148	198.2736
231	0.3536693191866	209.664
238	0.4597701149425	223.5744
245	0.4715590922487	239.5008
252	0.4420866489832	255.1248
259		
266	0.0589448865311	272.2608
273	0.0058944886531	273.3696
280	0.4067197170645	280.4256
287		
294	0.1002063071029	297.7632
301	0.218096080165	303.2064
308		
315	0.0884173297966	313.6896
322		
329		
336	0.106100795756	323.6688
343	0.3124078986148	330.8256
350		
357		
364	0.0589448865311	349.8768
371	0.3006189213086	356.0256
378	0.4244031830239	368.424
385	0.483348069555	383.9472



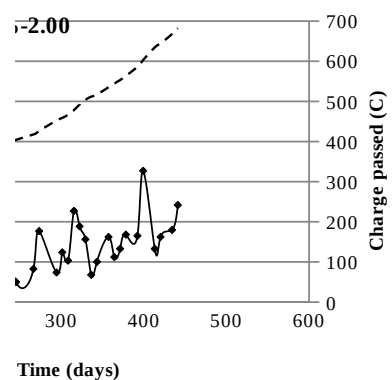
392	0.4479811376363	399.8736
399	0.4067197170645	414.4896
406	0.1532567049808	424.0656
413	0.2652519893899	431.2224
420		
427	0.1709401709402	446.1408
434	0.3713527851459	455.4144
441	0.3890362511052	468.4176
448	0.3890362511052	481.7232
455		
462	0.1532567049808	500.2704
469	0.4479811376363	510.552
476		
483	0.0707338638373	528.2928
490	0.159151193634	532.224
497		
504	0.0825228411435	540.4896
511	0.2947244326555	546.9408



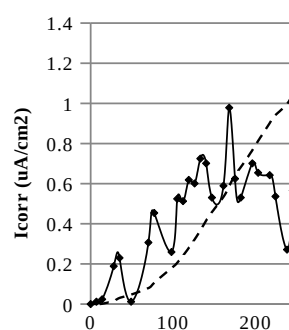
Time (day)	Icorr ( $\mu\text{A}/\text{cm}^2$ )	charge passed/C
0	0	0
7	0.1945181255526	3.3264
14	0.5069260241674	15.3216
28	0.2534630120837	41.328
35	0.3065134099617	50.904
42	0.2593575007368	60.5808
49	0.3300913645741	70.6608
56	0.7603890362511	89.3088
70	0.1414677276746	120.1536
77	0.0589448865311	123.5808
84	0.6896551724138	136.3824
98	0.106100795756	163.5984
105	0	165.4128
112	0.1827291482464	168.5376
119	0.0117889773062	171.864
126	0.3595638078397	178.2144
133	0.2829354553492	189.2016
140	0.1709401709402	196.9632
147	0.0117889773062	200.088
154	0.595343353964	210.4704
161	0.8134394341291	234.5616
168	0.5894488653109	258.552
175	0.9431181844975	284.76
182	0.8193339227822	314.8992
189		
196	0.0176834659593	343.5264
203	0.2004126142057	347.256
210	0.6071323312703	361.0656
217		
224	0.0648393751842	384.048
231	0.3006189213086	390.2976
238		
245	0.1002063071029	404.0064
252		
259		
266	0.1650456822871	417.6144
273	0.3536693191866	426.4848
280		
287		
294	0.1473622163277	452.1888
301	0.2475685234306	458.9424
308	0.2063071028588	466.704
315	0.4538756262894	477.9936
322	0.377247273799	492.2064
329	0.3124078986148	504
336	0.1355732390215	511.6608
343	0.2004126142057	517.4064
350		
357	0.324196875921	535.3488
364	0.2239905688182	544.7232
371	0.2652519893899	553.0896
378	0.3359858532272	563.3712
385		

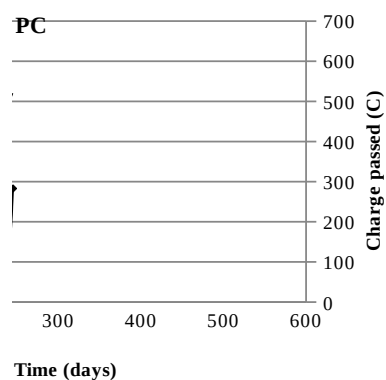


392	0.3300913645741	586.152
399	0.6542882404951	602.9856
406		
413	0.2652519893899	634.4352
420	0.324196875921	644.5152
427		
434	0.3595638078397	667.9008
441	0.483348069555	682.3152



Time (day)	Icorr (uA/cm <sup>2</sup> )	charge passed/C
0	0	0
7	0.0117889773062	0.2016
14	0.0235779546124	0.8064
21		
28	0.1886236368995	8.064
35	0.2298850574713	15.2208
42		
49	0.0117889773062	23.4864
56		
63		
70	0.3065134099617	39.816
77	0.4538756262894	52.8192
84		
91		
98	0.2593575007368	89.4096
105	0.5246094901267	102.816
112	0.5128205128205	120.5568
119	0.6189213085765	139.9104
126	0.6012378426172	160.776
133	0.7250221043325	183.456
140	0.70144414972	207.8496
147	0.5305039787798	228.9168
154		
161	0.5894488653109	267.2208
168	0.9784851164162	294.0336
175	0.6248157972296	321.4512
182	0.5305039787798	341.208
189		
196	0.70144414972	383.3424
203	0.6542882404951	406.5264
210		
217	0.6424992631889	450.8784
224	0.536398467433	471.0384
231		
238	0.271146478043	498.6576
245	0.5658709106985	527.5872

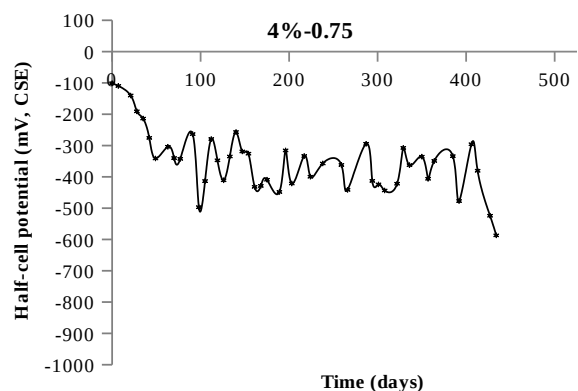








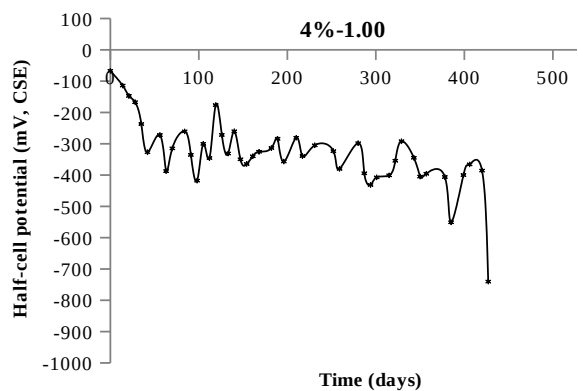
Time (day)	Potential (mV)
0	-101
7	-109.66666666667
21	-140.33333333333
28	-191
35	-214
42	-275.66666666667
49	-341.33333333333
63	-304
70	-340
77	-342.66666666667
91	-263.66666666667
98	-497
105	-413.66666666667
112	-279.33333333333
119	-347.33333333333
126	-411
133	-335
140	-257
147	-319
154	-326
161	-432
168	-429
175	-409.33333333333
182	
189	-448.33333333333
196	-315.66666666667
203	-421.33333333333
210	
217	-333.66666666667
224	-399.66666666667
231	
238	-357.33333333333
245	
252	
259	-362
266	-441.66666666667
273	
280	
287	-294.66666666667
294	-413
301	-424.33333333333
308	-443.66666666667
315	
322	-422
329	-307.66666666667
336	-362.66666666667
343	
350	-335.66666666667
357	-406.33333333333
364	-349.33333333333
371	
378	
385	-334



392 -477.3333333333  
399  
406 -296  
413 -380.6666666667  
420  
427 -524.3333333333  
434 -587

600

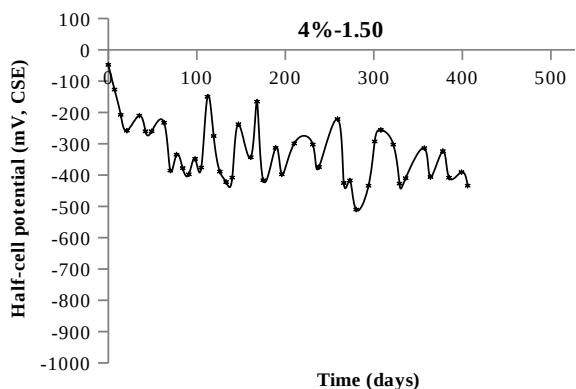
Time (day)	Potential (mV)
0	-67.333333333333
7	
14	-114.333333333333
21	-147.333333333333
28	-167.333333333333
35	-237
42	-327
56	-272.333333333333
63	-387.333333333333
70	-315
84	-260.666666666667
91	-335.666666666667
98	-418
105	-300.333333333333
112	-345.666666666667
119	-176.666666666667
126	-272
133	-331.333333333333
140	-260.333333333333
147	-349.666666666667
154	-364.666666666667
161	-340
168	-325.666666666667
175	
182	-313.666666666667
189	-284.333333333333
196	-357
203	
210	-281
217	-339.333333333333
224	
231	-305
238	
245	
252	-323.666666666667
259	-380.333333333333
266	
273	
280	-298.333333333333
287	-394.333333333333
294	-431.666666666667
301	-407.333333333333
308	
315	-401
322	-354.333333333333
329	-292
336	
343	-345
350	-405
357	-396
364	
371	
378	-406.333333333333



385	-551
392	
399	-400
406	-366
413	
420	-385.66666666667
427	-740.33333333333

600

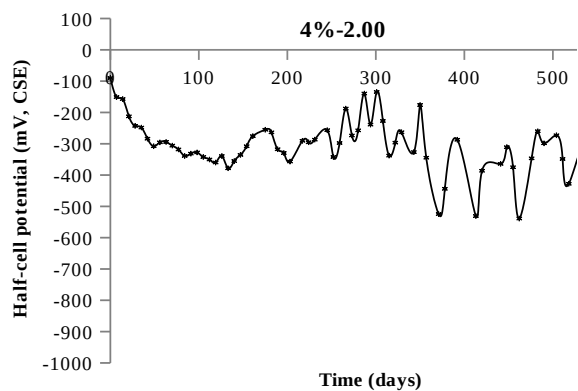
Time (day)	Potential (mV)
0	-48
7	-127
14	-207.666666666667
21	-258.333333333333
35	-210.333333333333
42	-260.333333333333
49	-260
63	-233
70	-385.666666666667
77	-335
84	-378
91	-397.666666666667
98	-348.666666666667
105	-376
112	-150
119	-275.333333333333
126	-389
133	-422.333333333333
140	-408.333333333333
147	-237.666666666667
154	
161	-343.333333333333
168	-165.666666666667
175	-416.666666666667
182	
189	-313
196	-397.666666666667
203	
210	-299.333333333333
217	
224	
231	-302.666666666667
238	-374.333333333333
245	
252	
259	-221.333333333333
266	-425.333333333333
273	-417.333333333333
280	-510.333333333333
287	
294	-434
301	-292.666666666667
308	-256
315	
322	-302.666666666667
329	-427.333333333333
336	-410
343	
350	
357	-314
364	-406.333333333333
371	
378	-323.666666666667



385 -408.3333333333  
392  
399 -390.66666666667  
406 -434

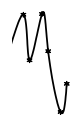
600

Time (day)	Potential (mV)
0	-90
7	-151
14	-157.333333333333
21	-212.666666666667
28	-243
35	-248.333333333333
42	-284
49	-308
56	-295.666666666667
63	-294.333333333333
70	-306
77	-318.333333333333
84	-339
91	-331.666666666667
98	-327.666666666667
105	-342.333333333333
112	-350.333333333333
119	-360
126	-339.333333333333
133	-378.333333333333
140	-355.333333333333
147	-335.666666666667
154	-308
161	-275.666666666667
175	-255.333333333333
182	-263.666666666667
189	-317.666666666667
196	-329.666666666667
203	-357
217	-290.666666666667
224	-295.333333333333
231	-287
245	-256.666666666667
252	-342.333333333333
259	-297.666666666667
266	-187.666666666667
273	-273.666666666667
280	-257.333333333333
287	-139.666666666667
294	-239
301	-134.666666666667
308	-227.333333333333
315	-338
322	-296.666666666667
329	-263.333333333333
336	
343	-326.666666666667
350	-176.333333333333
357	-344.666666666667
364	
371	-524.666666666667
378	-444
385	

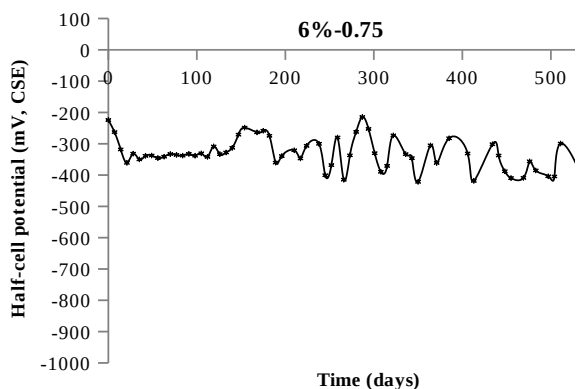


392 -287.3333333333  
399  
406  
413 -531  
420 -386.3333333333  
427  
434  
441 -364.3333333333  
448 -311  
455 -375  
462 -539  
469  
476 -346.6666666667  
483 -260  
490 -298.6666666667  
497  
504 -273  
511 -348.6666666667  
518 -428  
525  
532  
539 -277.6666666667  
546 -423  
553  
560 -275.3333333333  
567 -394  
574  
581 -588.3333333333  
588 -498.3333333333

600



Time (day)	Potential (mV)
0	-224.33333333333
7	-263
14	-318.33333333333
21	-361
28	-331.66666666667
35	-350
42	-338.66666666667
49	-337.66666666667
56	-345.66666666667
63	-341.33333333333
70	-333
77	-335.66666666667
84	-338
91	-332.66666666667
98	-338.33333333333
105	-330.66666666667
112	-342
119	-308.66666666667
126	-333.33333333333
133	-328
140	-313
147	-271
154	-248.66666666667
168	-263.66666666667
175	-258.66666666667
182	-274.66666666667
189	-360.33333333333
196	-339.33333333333
210	-321
217	-347
224	-306.66666666667
238	-300.33333333333
245	-400.66666666667
252	-368.33333333333
259	-280
266	-415
273	-337
280	-262.33333333333
287	-214.66666666667
294	-252.66666666667
301	-330.33333333333
308	-389.66666666667
315	-371
322	-273.33333333333
329	
336	-333.33333333333
343	-346
350	-421.66666666667
357	
364	-305.33333333333
371	-361.33333333333
378	
385	-282.66666666667



392  
399  
406 -331.33333333333  
413 -418.66666666667  
420  
427  
434 -301.66666666667  
441 -337.66666666667  
448 -388  
455 -409.66666666667  
462  
469 -409  
476 -356.33333333333  
483 -385.33333333333  
490  
497 -404  
504 -404.66666666667  
511 -299.33333333333  
518  
525  
532 -389.33333333333  
539 -426  
546  
553 -347.66666666667  
560 -428  
567  
574 -576.33333333333  
581 -422.33333333333

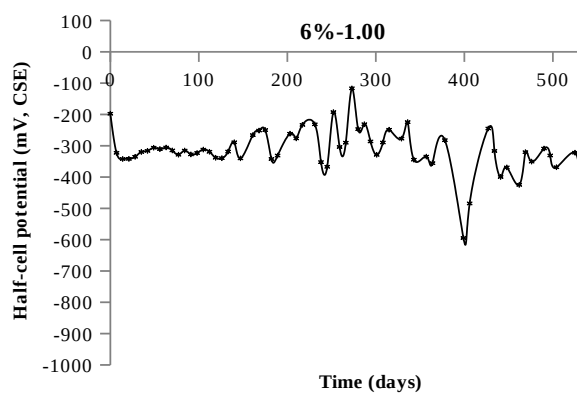


600



V

Time (day)	Potential (mV)
0	-197.666666666667
7	-322.666666666667
14	-342.333333333333
21	-342
28	-335.333333333333
35	-320
42	-316.333333333333
49	-306.333333333333
56	-310.666666666667
63	-305.666666666667
70	-315
77	-328.666666666667
84	-315.333333333333
91	-327.666666666667
98	-323.333333333333
105	-312.333333333333
112	-319.333333333333
119	-338.333333333333
126	-339.666666666667
133	-318.666666666667
140	-289
147	-340.333333333333
161	-266
168	-251.666666666667
175	-250
182	-342.333333333333
189	-331.333333333333
203	-261.666666666667
210	-276.666666666667
217	-233.333333333333
231	-231.666666666667
238	-352.333333333333
245	-367.333333333333
252	-192.666666666667
259	-304
266	-290.333333333333
273	-116.666666666667
280	-247
287	-231.333333333333
294	-286.333333333333
301	-329
308	-289.666666666667
315	-249
322	
329	-277.333333333333
336	-224.666666666667
343	-344.666666666667
350	
357	-334.666666666667
364	-355.666666666667
371	
378	-282.333333333333
385	



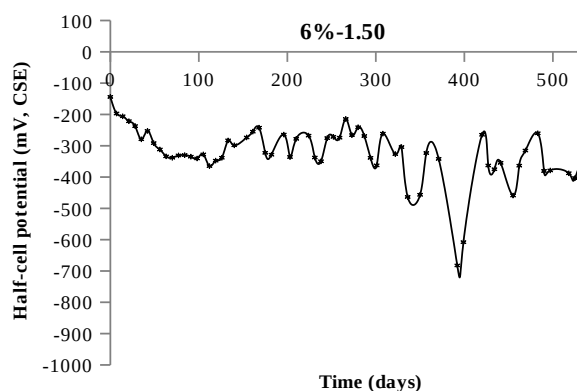
392  
399 -594.66666666667  
406 -484.33333333333  
413  
420  
427 -245  
434 -316.66666666667  
441 -399.66666666667  
448 -369.33333333333  
455  
462 -425  
469 -320.66666666667  
476 -350.66666666667  
483  
490 -309  
497 -331  
504 -368.66666666667  
511  
518  
525 -322.33333333333  
532 -394  
539  
546 -315  
553 -433.33333333333  
560  
567 -721  
574 -453.66666666667



600



Time (day)	Potential (mV)
0	-144
7	-197
14	-206
21	-221.66666666667
28	-237.33333333333
35	-279.33333333333
42	-252.66666666667
49	-291.66666666667
56	-312
63	-334
70	-338.33333333333
77	-331
84	-330
91	-335
98	-340.66666666667
105	-327.66666666667
112	-365
119	-347.66666666667
126	-338.33333333333
133	-283
140	-298.66666666667
154	-273.66666666667
161	-255
168	-242.33333333333
175	-322.66666666667
182	-328.66666666667
196	-264.33333333333
203	-336
210	-278
224	-267.66666666667
231	-337.66666666667
238	-349.66666666667
245	-275.66666666667
252	-271.66666666667
259	-274.33333333333
266	-214.66666666667
273	-266
280	-241
287	-269
294	-338.66666666667
301	-362.66666666667
308	-261.33333333333
315	
322	-326.66666666667
329	-304.33333333333
336	-463.66666666667
343	
350	-456.66666666667
357	-323.33333333333
364	
371	-342
378	
385	



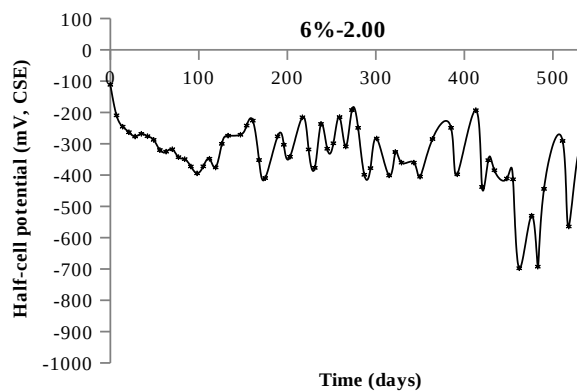
392	-682.33333333333
399	-608
406	
413	
420	-265
427	-363
434	-375
441	-354.66666666667
448	
455	-459
462	-363.66666666667
469	-315.33333333333
476	
483	-260.33333333333
490	-380.66666666667
497	-379
504	
511	
518	-388
525	-403.33333333333
532	
539	-299.66666666667
546	-371
553	
560	-491.33333333333
567	-492



600



Time (day)	Potential (mV)
0	-111.666666666667
7	-209.333333333333
14	-245.666666666667
21	-263.333333333333
28	-277
35	-268.333333333333
42	-276
49	-287.666666666667
56	-320.333333333333
63	-325.333333333333
70	-317.666666666667
77	-343
84	-349.333333333333
91	-372.666666666667
98	-394.666666666667
105	-372.333333333333
112	-348
119	-375.666666666667
126	-300.333333333333
133	-274.333333333333
147	-271.333333333333
154	-242
161	-226.333333333333
168	-352
175	-409.666666666667
189	-276.333333333333
196	-303.333333333333
203	-341.666666666667
217	-215.666666666667
224	-318.333333333333
231	-377
238	-237
245	-316
252	-298.666666666667
259	-215
266	-309
273	-192.333333333333
280	-249.333333333333
287	-399
294	-378
301	-283.333333333333
308	
315	-401.333333333333
322	-326.333333333333
329	-360.333333333333
336	
343	-360.333333333333
350	-405.333333333333
357	
364	-285
371	
378	
385	-249.333333333333



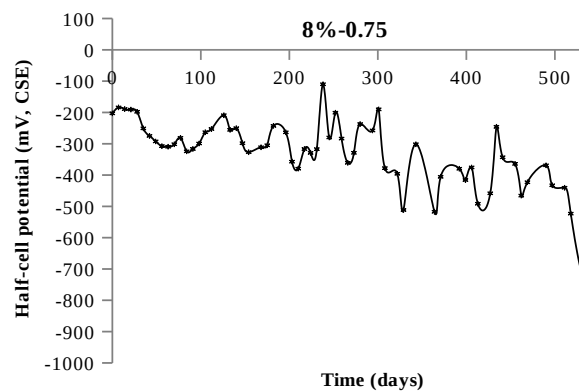
392 -397.66666666667  
399  
406  
413 -193  
420 -438  
427 -352.66666666667  
434 -384.66666666667  
441  
448 -411  
455 -413.66666666667  
462 -697.66666666667  
469  
476 -530  
483 -692.66666666667  
490 -444.33333333333  
497  
504  
511 -291  
518 -564.33333333333  
525  
532 -334.66666666667  
539 -894.33333333333  
546  
553 -389  
560 -432



600



Time (day)	Potential (mV)
0	-203
7	-184
14	-189.333333333333
21	-191
28	-198
35	-251
42	-275
49	-292.666666666667
56	-307.666666666667
63	-309.666666666667
70	-301.666666666667
77	-281.333333333333
84	-324.333333333333
91	-316.666666666667
98	-299.333333333333
105	-263.333333333333
112	-253
126	-209
133	-255.666666666667
140	-250.333333333333
147	-298.333333333333
154	-327
168	-311.333333333333
175	-305
182	-243
196	-263.666666666667
203	-357.333333333333
210	-379.666666666667
217	-317
224	-329.333333333333
231	-317.333333333333
238	-110
245	-280
252	-201
259	-283.666666666667
266	-361
273	-329
280	-237.333333333333
287	
294	-257.666666666667
301	-190.333333333333
308	-378
315	
322	-396
329	-511.666666666667
336	
343	-301.666666666667
350	
357	
364	-517.333333333333
371	-405.666666666667
378	
385	

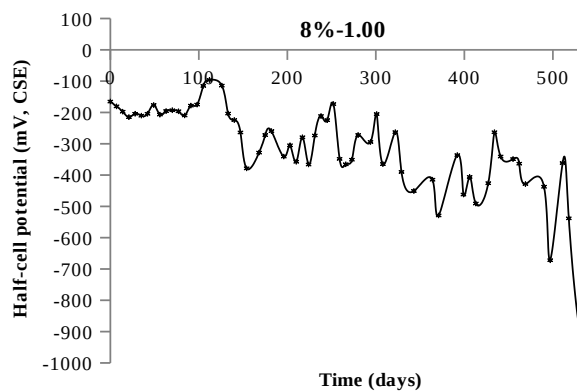


392	-380
399	-416
406	-375.666666666667
413	-491.666666666667
420	
427	-458.33333333333
434	-246
441	-343.33333333333
448	
455	-364.33333333333
462	-465.666666666667
469	-423
476	
483	
490	-369
497	-432.666666666667
504	
511	-440.666666666667
518	-523.33333333333
525	
532	-727
539	-618.666666666667

600

J

Time (day)	Potential (mV)
0	-165.333333333333
7	-180.666666666667
14	-197.666666666667
21	-215
28	-204.333333333333
35	-210.333333333333
42	-204.333333333333
49	-176.333333333333
56	-207
63	-195.666666666667
70	-193
77	-196.333333333333
84	-209.666666666667
91	-178.333333333333
98	-175
105	-115.333333333333
112	-96.333333333333
126	-114.333333333333
133	-203.666666666667
140	-224.333333333333
147	-264
154	-378.666666666667
168	-328.333333333333
175	-272.333333333333
182	-259.666666666667
196	-341
203	-305
210	-357.666666666667
217	-279.333333333333
224	-366.333333333333
231	-273.666666666667
238	-211.666666666667
245	-224.666666666667
252	-173.333333333333
259	-348.333333333333
266	-365.666666666667
273	-351
280	-272.333333333333
287	
294	-294.333333333333
301	-205.333333333333
308	-365
315	
322	-263
329	-390
336	
343	-451
350	
357	
364	-415
371	-529
378	
385	

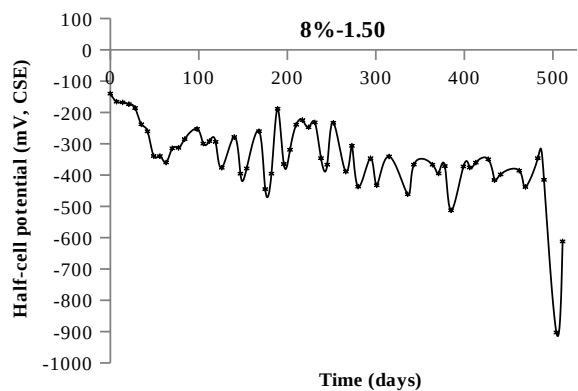


392 -336.3333333333  
399 -462.3333333333  
406 -406  
413 -491  
420  
427 -426  
434 -263.3333333333  
441 -341  
448  
455 -349  
462 -363.6666666667  
469 -428.6666666667  
476  
483  
490 -437.3333333333  
497 -672  
504  
511 -361.6666666667  
518 -538.3333333333  
525  
532 -917  
539 -676

600

J

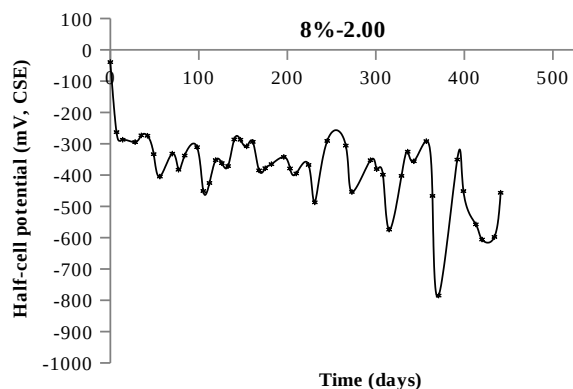
Time (day)	Potential (mV)
0	-140
7	-165.666666666667
14	-168
21	-173.666666666667
28	-186
35	-238
42	-260.333333333333
49	-339.333333333333
56	-339.666666666667
63	-360
70	-314.666666666667
77	-313
84	-285.333333333333
98	-253
105	-299.666666666667
112	-291.666666666667
119	-294
126	-376.666666666667
140	-278.666666666667
147	-395.666666666667
154	-379
168	-260
175	-445
182	-395.666666666667
189	-188.333333333333
196	-365
203	-319.333333333333
210	-239.333333333333
217	-224.666666666667
224	-247.333333333333
231	-232
238	-346
245	-367
252	-233
259	
266	-389
273	-306.666666666667
280	-437
287	
294	-346.333333333333
301	-432.666666666667
308	
315	-340.666666666667
322	
329	
336	-461.333333333333
343	-366.666666666667
350	
357	
364	-367
371	-395
378	-371.333333333333
385	-512.666666666667



392  
399 -372.66666666667  
406 -376  
413 -360.33333333333  
420  
427 -349.66666666667  
434 -416  
441 -398  
448  
455  
462 -386  
469 -438  
476  
483 -346  
490 -415.33333333333  
497  
504 -903  
511 -612

600

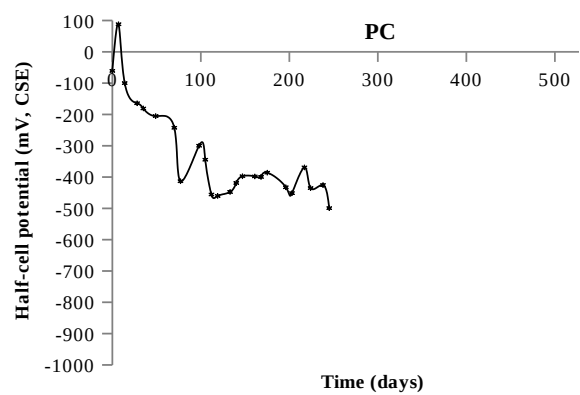
Time (day)	Potential (mV)
0	-39.333333333333
7	-263
14	-287.333333333333
28	-294.666666666667
35	-273.333333333333
42	-274.666666666667
49	-333.333333333333
56	-405
70	-331.666666666667
77	-383
84	-337.666666666667
98	-311
105	-451
112	-425.333333333333
119	-352.333333333333
126	-362
133	-371.333333333333
140	-286.333333333333
147	-287.333333333333
154	-308.333333333333
161	-294
168	-385
175	-378.333333333333
182	-365.333333333333
189	
196	-342.333333333333
203	-379
210	-395
217	
224	-367.666666666667
231	-487.333333333333
238	
245	-291
252	
259	
266	-306
273	-454
280	
287	
294	-352.666666666667
301	-381
308	-399
315	-574.333333333333
322	
329	-402.666666666667
336	-325.333333333333
343	-356
350	
357	-291.666666666667
364	-466.666666666667
371	-785
378	
385	



392 -350.66666666667  
399 -451.33333333333  
406  
413 -557.66666666667  
420 -606  
427  
434 -597.66666666667  
441 -456.66666666667

600

Time (day)	Potential (mV)
0	-61
7	88
14	-100
21	
28	-164.333333333333
35	-181
42	
49	-205.333333333333
56	
63	
70	-242.666666666667
77	-413.333333333333
84	
91	
98	-300
105	-344.666666666667
112	-455.666666666667
119	-460.333333333333
126	
133	-447.666666666667
140	-419
147	-397.333333333333
154	
161	-398
168	-399.666666666667
175	-386
182	
189	
196	-432.666666666667
203	-451.333333333333
210	
217	-369.333333333333
224	-435.333333333333
231	
238	-425.666666666667
245	-499.333333333333



600